2013

Psychological Behavior Analysis Using Advanced Signal Processing Techniques for fMRI Data

Charisma Dionne Edwards
Louisiana State University and Agricultural and Mechanical College, cedwa15@tigers.lsu.edu

PSYCHOLOGICAL BEHAVIOR ANALYSIS USING ADVANCED SIGNAL PROCESSING TECHNIQUES FOR FMRI DATA

A Dissertation

Submitted to the Graduate Faculty of the
Louisiana State University and
Agricultural and Mechanical College
in partial fulfillment of the
requirements for the degree of
Doctor of Philosophy

in

The School of Electrical Engineering and Computer Science

by
Charisma D. Edwards
B.S., Clark Atlanta University, 2004
M.S., Louisiana State University, 2007
December 2013

Acknowledgements

First, I would like to reverence my Creator, Savior, and Comforter who renews my strength, wisdom, and courage daily. Because of you, I am who I am. A lifetime of words cannot express my deepest gratitude. May all that I do with the blessings you have provided be pleasing to you, and may the fruit I bear speak for me.

To my major professor and dissertation advisor, Dr. Hsiao-Chun Wu, thank you so much for all that you do! You have been most patient, encouraging, and understanding throughout this entire process. Moreover, you have helped me to grow as an independent researcher, and I greatly appreciate you for that. I am grateful for our many conversations and for your mentorship, guidance, leadership, and coaching throughout my graduate career.

Also, I thank my committee individually and collectively: Dr. Bahadir Gunturk, Dr. Xuebin Liang, Dr. Frank Neubrander, and Dr. James Van Scotter as well as my special mentors: Dr. Theda Daniels-Race, Dr. Zakiya Wilson, Dr. Vaneshette Henderson, Dr. Su-Seng Pang, Dr. Marco Barker, and Dr. Saundra McGuire. I am grateful for your confidence in me, critiques and assistance throughout my graduate career. I have learned so much from each of you, and I could not have done this without you. Thank you so much for your time and service.

Thank you to the Wu research group throughout my tenure: Dr. Sameer Herlekar, Dr. Xiaozhou Huang, Mr. Kiran Mada, Mr. Waheeduddin Syed, Mr. Srinath Sitaraman, Mr. James Thomas, Ms. Songnan Xi, Dr. Kun Yan, Dr. Lu Lu, Dr. Xiaoyu Feng, Dr. Yonas Debessu, Mrs. Hongting Zhang, and Mr. Tian Xia. I appreciate each of you, and I wish you all the best. A special thank you goes to Visiting Professor, Dr. Limei Guo for your hard

work and assistance with this research. I truly appreciate you taking the time to help me. To my undergraduate research students, Daniel Miles, Vilien Gomez, and Alexander Canton, thank you for helping me to develop as a research mentor.

I would be remised if I did not acknowledge the National Science Foundation, who has sponsored my entire post-secondary education in one form or another through the LS-AMP grants, GK-12 grant, and now, NSF/Innovation through Institutional Integration (I^3) Graduate Assistantship. Additionally, I would like to thank the Brentwood Community Foundation of Houston, Texas for the Lionel Thompson Memorial Scholarship and the Rodney and Marion Wilson Engineering Scholarship and the Shiloh Missionary Baptist Church for the Winstonia Smith Memorial Scholarship. To the LSU College of Engineering, thank you so much for the Donald W. Clayton Graduate Award.

Many thanks go to Dr. Isiah Warner and the Office of Strategic Initiatives, the College of Engineering Office of Diversity Programs (formerly Minority Engineering Program headed by Mrs. Cheryle Peters), the Office of Multicultural Affairs, Black Graduate & Professional Student Association, and Shiloh Missionary Baptist Church for keeping me funded and developing me in leadership, teaching, and service. You each have believed in me, supported constant growth in various ways, and helped me to develop further than I would have ever imagined. Moreover, through your programs, I have increased my network tremendously and have developed lifelong friendships.

To my Clark Atlanta University family, thank you for laying my foundation and for inspiring and even expecting me to pursue doctoral studies. Specifically, I want to thank the PRISM-D/GA-LS-AMP fellowship program including Dr. Melvin Webb, Ms. Jacqueline Jackson, the late Ms. Gwen Sapp and the late Dr. Gwen Johnson; Honors

Program under the leadership of Dr. Isabella T. Jenkins; Department of Engineering; and my CAU Cheerleaders under the watchful care of Valerie “Momma” Jordan. To my undergraduate advisor, Dr. Musa Danjaji, thank you for being unrelenting in your demand for academic excellence. Because of you, I have reached this milestone.

Finally, my sincerest appreciation goes to my mother, Beverly Cooper for giving so much of yourself for me. To my father, Kirk Edwards, Sr. thank you for a lifetime of learning. To my step-father, Charles Cooper, Sr., thank you for teaching me to move slowly and be patient. To my brothers, Kirk, Jr. and “CJ”, I could not have asked for more loving and fun brothers. To my fiancé, Samuel L. Milledge, II, I love you from the depths of my soul. Our talks have gotten me through the most difficult times. Keep it coming. To all of my family and friends (too numerous to name), biological and extended along with the village that raised me, I appreciate your unfailing love, support, and prayers. I hope to continually make you proud, and I hope to positively impact many more to come. I love you all!

Table of Contents

List of Figures

Abstract

Psychological analysis related to voluntary reciprocal trust games were obtained using functional magnetic resonance imaging (fMRI) hyperscanning for 44 pairs of strangers throughout 36 trust games (TG) and 16 control games (CG). Hidden Markov models (HMMs) are proposed to train and classify the fMRI data acquired from these brain regions and extract the essential features of the initial decision of the first player to trust or not trust the second player. These results are evaluated using the different versions of the multifold cross-validation technique and compared to other speech data and other advanced signal processing techniques including linear classification, support vector machines (SVMs), and HMMs. With above 80% classification accuracy for HMM as compared to no more than 66% classification accuracy of a linear classifier and SVM, the corresponding experimental results demonstrate that the HMMs can be adopted as an outstanding paradigm to predict the psychological financial (trust/non-trust) activities reflected by the neural responses recorded using fMRI. Additionally, extracting the specific decision period and clustering the continuous time series proved to increase the classification accuracy by almost 20%.

1. Motivation

"A social instinct is implanted in all men by nature …" – Aristotle, Politics, Book I [3] The human sciences such as sociology, anthropology, psychology and others have long studied intelligent behavior [4]. Humans have a unique, innate capacity to perceive, learn and adapt to their surroundings [5]. Because of shared space between people, cooperative and interdependent relationships tended to develop as a means to navigate society. Consistent with the Merriam-Webster, Incorporated dictionary, these relationships are social in nature. According to Fortune Magazine almost a decade ago, "alliances have become an integral part of contemporary strategic thinking" [6]. Partnerships, when formed carefully and methodically, make individuals and entire entities more efficient and thus, more competitive. This collaboration is beneficial because of the alternative perspectives offered and the reduced demand for resources.

1.1 Social Intelligence

Social interactions are critical to how we see the world. Social rules help to recognize probable behavioral patterns and respond accordingly. To effectively handle these often complex social situations, one must be able to observe, understand and react to social cues manifested in subtle expressions and body language as well as prolonged behaviors. This may be termed as *social intelligence* [5, 7]. Social intelligence can be more specifically defined as the ability to manage, express and recognize turn-taking, agreement, politeness, empathy, cooperation and other social signals, behaviors and situations [5]. The goal of social intelligence is to *perceive*, *interpret* and *display* appropriate social signals and behavior [4].

True feelings and attitudes towards social interactions and situations are often expressed in social signals, though sometimes unconsciously [4]. These signals include interest, friendliness, determination, boredom, activity, engagement, emphasis, emulating and other attitudes toward a particular social situation. Effective teachers and speakers often use these signals such as posture to gauge the attentiveness of the audience. As Pentland phrased it, "signaling functions as a subconscious discussion about relationships, resources, risks, and rewards" [8], and oftentimes, the unspoken signals are just as important as the spoken words. One could venture to say that the unspoken signals are more important because of their involuntary nature.

Pentland also writes about the importance of social signals in predicting human behavior. Social psychologists employ this expertise in school, business, government, and family situations. Expert psychologists can quite accurately forecast important life events such as divorce, student performance or criminal conduct after a short period of observation although these events may not occur in the immediate future [8, 9]. Another benefit to monitoring social signals may be in improving group function. Facilitators or moderators can provide real-time intervention based on behavioral signals and social cues such as physical appearance, gestures, posture, face and eye behavior, vocal behavior and space and environment [8]. Given the subconscious nature of many social signals, all behaviors are not robustly detectable using conventional methods like audio-visual recording. There is a greater need to view the subconscious in more depth on a neurological level.

Neuroscience offers a balance between biological and psychological approaches to social behavior. The idea is that neural regulation reflects a simple contrast. On the one hand, there are innate, automatic processes that are not affected by perception or reasoning.

On the other hand, we have learned behaviors that are more controlled and methodical and depend upon contexts or situations. Certain physiological components have even been identified to improve the awareness of others or to process and influence even the most complex judgments such as whether or not to trust other people [4, 10].

1.2 Social Signal Processing

In a society that is becoming more mobile and globally interactive with increasing human-technology interfacing and computer-mediated communication, systems that detect and measure social signals and behavioral cues will prove to be advantageous. These signals can be detected through verbal, facial, body, physiological or other characteristics. Such "socially aware" systems could even detect attitudes during negotiation for example. In the case of group function, social scientists have researched how groups of people make decisions and the effects of social environments on these group relations. Impressions of dominance, authority, respect or affinity can impact social interactions. By understanding the relationship between social signaling and behavior, outcomes can be predicted. In order to do so, the goal must be to detect, interpret and classify signals and how they affect behavior [8, 9, 11, 12].

To address this crucial issue, there is growing interest in the multidisciplinary research field of *social signal processing* (SSP, also associated with *behavioral* or *cognitive signal processing*) [4, 5, 7, 8, 11-17]. This field is defined by Vinciarelli *et al.* as "*machine analysis of human social signals*" [5] and related to behaviors obtained from physical appearance, gestures and posture, face and eye behavior, vocal behavior, space and environment. It is an intriguing method of automating the human-intelligent process of perceiving, learning and adapting to social situations. It is a product of artificial intelligence

and socially aware computing. Social signal processing applications range from psychological coaching or diagnosis to more engaging games or technology. Most often, these behavioral signals and social cues are detected with audio and/or video equipment. However, recent developments have utilized neurological "hyperscanning" to detect this information although it is more invasive [5, 11]. This hyperscanning will be discussed in more detail in Section 1.3

Social signal processing has also gained notoriety for its use in context-dependent human-computer interactions [5]. The major components of SSP are *modeling*, *analysis* and *syntheses* of nonverbal behaviors in social interactions. The modeling component observes underlying rules that govern social interaction and the effects of nonverbal behaviors. The analysis component examines the automatic techniques used to extract and interpret data recorded during social interaction from appropriate sensors usually microphones for audio signals and cameras for nonverbal behavioral cues. The synthesis

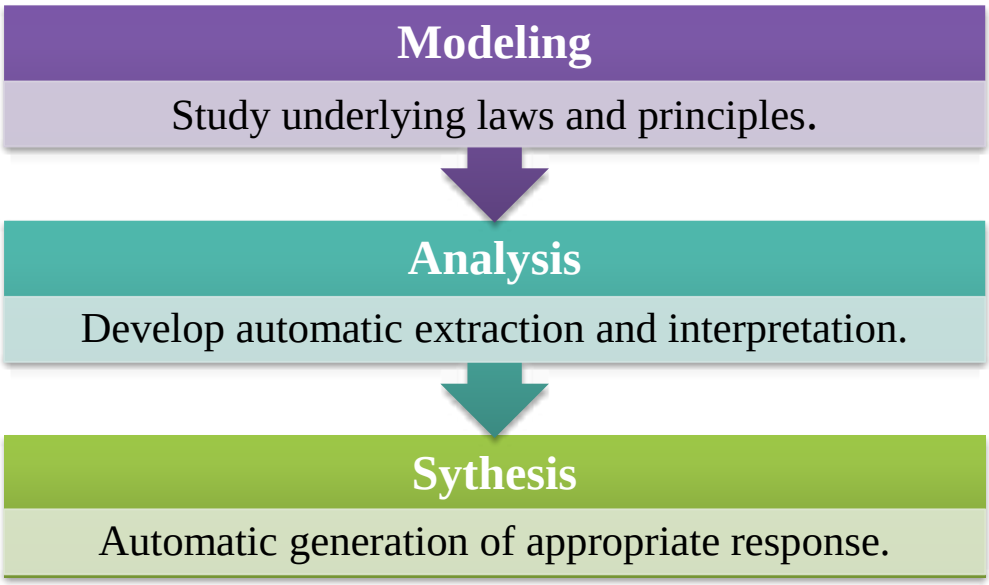

Figure 1. Graphical representation of social signal processing components.

Figure 2. Graphical representation of Analysis component of social signal processing.

component explores the process of automatically generating a suitable response as deemed by social laws and principles and in proper context. A summary of these components is represented graphically in Figure 1 [4]. The analysis component, which is most relevant to the scope of this research, can further be divided as in Figure 2. The first phase of analysis is recording of the social scene like meetings and other interactions in which the social signals and behaviors may be extracted. In order to extract these social cues using various techniques appropriate to the signal of interest, the people involved in the interaction must first be detected. Finally, it is equally important to sense the context of the scene in order to properly classify signals [4].

1.3 Hyperscanning with fMRI

Using *functional magnetic resonance imaging* (fMRI), some neuroeconomics research has studied social decision making. The interest is how decisions are influenced when others are also making decisions and/or are affected by the result [18]. This research employs von Neuman's game theory [19, 20] to develop experiments and interpret results. Specifically, researchers are interested in the neural sequences that correspond to particular outcomes. To further investigate what occurs physiologically as two people attempt to sense and influence what each other is doing, it is best to record or measure this activity simultaneously. This "hyperscanning" is a method of measuring brain activity during social

interaction. Although social behavior can be subtle, neuroscientists have made some advancement in identifying parts of the brain that are the basis for these social interactions. However, specific patterns and implications of neural activation are still being explored [2, 10, 18, 21].

Functional magnetic resonance imaging has become a prevalent technique used across multidisciplinary research to investigate brain activity in response to a stimulus or task. Its growing popularity is partly attributable to its accessibility, non-invasive nature, and high spatial and temporal resolutions [22]. It can provide insight into the functioning of sensory, motor and cognitive systems through detailed images of the human brain that reflect local changes in blood dynamics [1]. The three main components of fMRI, namely data acquisition, data processing and analysis, and interpretation, relate to specific conceptual and technical developments as well as scientific disciplines [23].

In the fMRI acquisition component, the scan type or pulse sequence is sensitive to blood dynamics. The measurements of these changes in blood dynamics such as blood flow, volume and oxygenation state, indicate changes in neural activity [22]. The most common method, blood-oxygenation-level-dependent (BOLD) contrast, measures a decrease in the local concentration of deoxyhemoglobin caused by the presence of more oxygenated blood needed in the area of the brain responsible for reacting to a specific stimulus or task. This decrease in deoxyhemoglobin reduces the magnetic field distortions, which slightly intensifies the magnetic resonance (MR) signal [24, 25]. De Yoe *et al.* illustrated this process with the detailed flowchart shown in Figure 3 (see [1]).

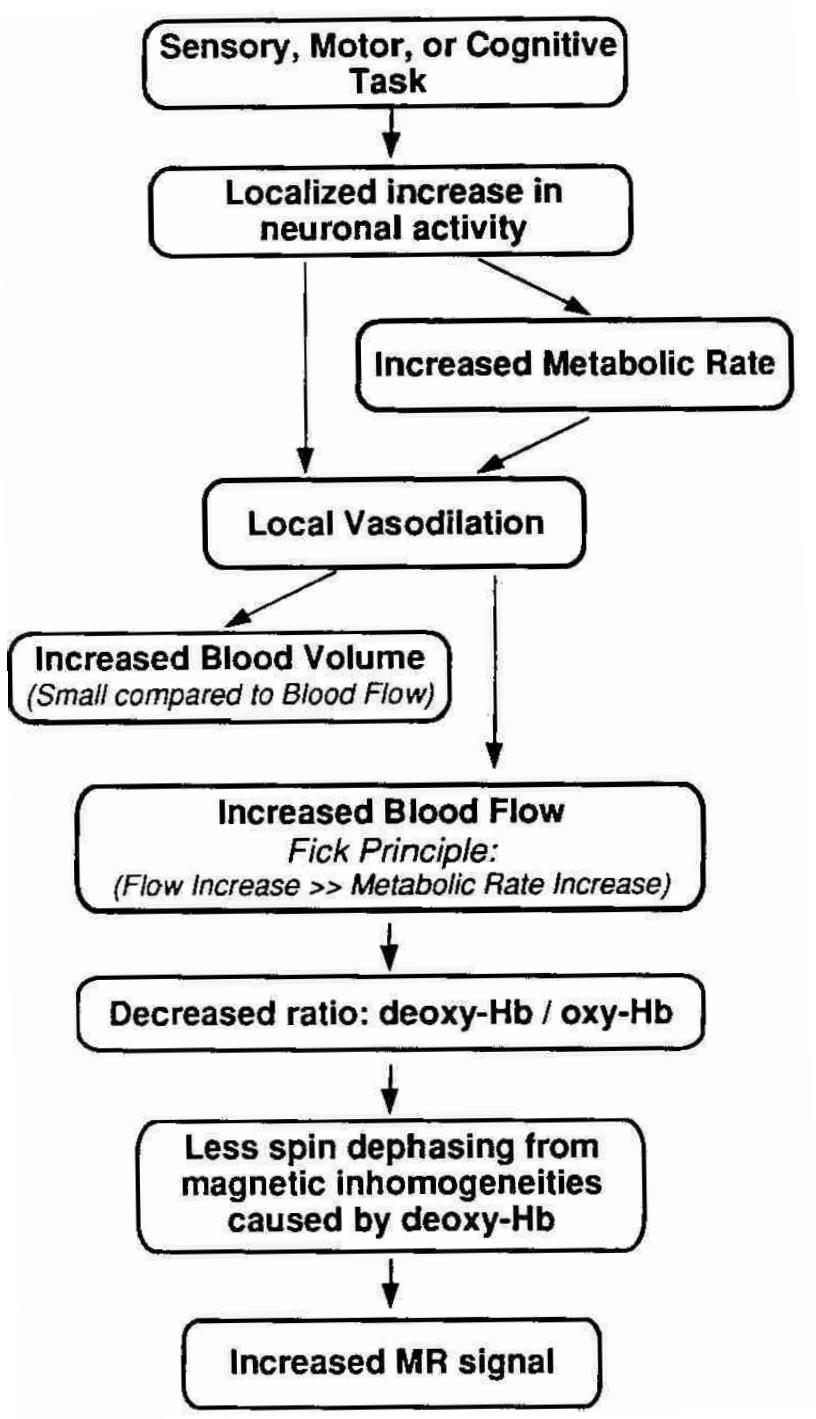

Figure 3. Reused from [1]. See permissions in Appendix A. "Hypothesized mechanism of BOLD contrast underlying common fMRI approaches (Hb ≡ hemoglobin)".

The data processing and analysis component attempts to detect the changes in signal intensities. The objectives are (*i*) to quantify relationships between task characteristics, MR signals and regions and/or identify which brain regions are included in the function of interest (FOI), and (*ii*) to extract the function-related signal changes optimally by minimizing noise and variability [23]. Generally, there are two types of approaches: confirmatory (hypothesis- or model-driven) and exploratory (data-driven) [24-27], but more recently, clustering methods such as hierarchical clustering have emerged as yet another valid category of fMRI analysis methods [25]. The confirmatory approaches are classified according to the necessity of *a priori* knowledge about the experimental paradigm. Some of the most popular analysis programs currently available, e.g. SPM (www.fil.ion.ucl.ac.uk/spm), Brain Voyager (www.brainvoyager.de) and AFNI (afni.nimh.nih.gov/afni), use multiple regression analysis to assign statistical significance to changes in the fMRI signal associated with the task. Some other programs employ connectivity analysis, which test for correlations between regions while others employ independent or principal component analysis, which extract main factors in the data time series [23].

The experimental paradigm, i.e., design of the task or stimulus, presented during scanning influences how the results should be interpreted. Carefully chosen experimental paradigms facilitate the search for and identification of regions involved in the FOI. This allows for testing of the regional effects of variations in the experiment [23]. An exceptional graphical layout of the aforementioned fMRI components is shown in Figure 4 (obtained from [1, 28]).

.

Figure 4 (next page). Reused from [1]. See permissions in Appendix A. "Example of results of post-processing of responses in visual cortex to alternations of baseline and experimental tasks. (A) multigraph display of the time course of the fMRI signal from 25 voxels located near the occipital pole in the primary visual cortex. The 200-second scan duration is represented by the width of each square in the multigraph display. Note the cyclic responses to 5 alternations of a uniform blank field (stimulus off) with a counterphase flickered (8Hz), checkered annulus of 6° diameter centered on a small fixation point. (B) Average reference wave form computed from 10 selected pixels. (C) Correlation image (axial view) showing the degree of correlation between the reference wave and the response from each voxel in the slice. Color scale represents positive correlations in red/yellow, negative correlations by blues. (D) Distribution of correlation coefficients from a blank series (control task only, no alternation). Red curve shows Gaussian function fitted to data. (E) Distribution of correlation coefficients taken from experimental scan represented by image C. Valid response criteria for both positive and negatively correlated responses shown by red arrows. (F) Sagittal view of brain showing plane of functional images (POS: parieto-occipital sulcus). (G) Composite functional images (axial view) for different correlation criteria shown by the number next to each image. Color scale for functional data codes the magnitude of the reference wave form represented by the original data from each voxel. As correlation threshold increases, confidence in the validity of the displayed foci increases. For this case, a threshold of 0.65 yielded a probability of false-positive response of $P < 0.001$ (case CT)."

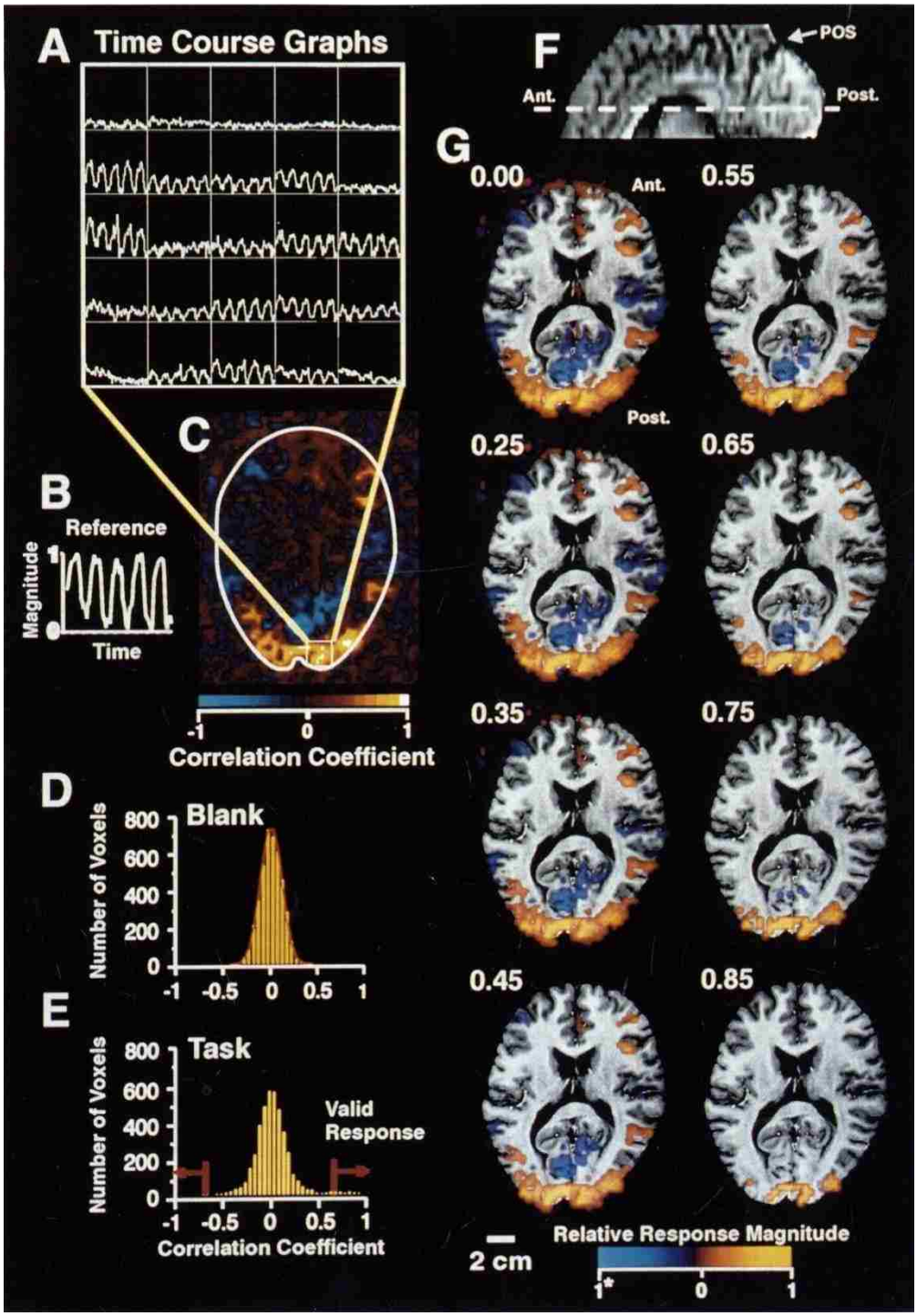
A
Time Course Graphs
B
Reference
Magnitude
1
Time
C
-1
0
1
Correlation Coefficient
D
Blank
Number of Voxels
800
600
400
200
0
-1
-0.5
0
0.5
1
E
Task
Valid
Response
Correlation Coefficient
F
POS
Ant.
Post.
G
0.00
Ant.
0.55
Post.
0.25
0.65
0.35
0.75
0.45
0.85
2 cm
Relative Response Magnitude
1*
0
1

Chapter 2 will state the problem followed by an exploration of the current status of knowledge on the subject matter in Chapter 3. Then, we will present our approach and experimental results in Chapters 4 and 5, respectively. Finally, the conclusion will be drawn in Chapter 6.

2. Problem Statement

Neuroeconomics researchers have determined that trust and cooperation are vital in human social behavior. Moreover, recent studies have concluded that these sentiments are essential to economic decision-making [2, 18-20]. Using the aforementioned hyperscanning, Krueger *et al.* has studied neural connections involved with the trust and cooperation of personal economic exchange by simultaneously scanning the brains of two players active in a voluntary reciprocal trust game. After analysis of the results, they concluded that the brain activity involved in developing a trusting relationship is concentrated primarily in the paracingulate cortex (PcC). More specifically, the ventral tegmental area (VTA, linked to the evaluation of expected and attained reward) and the septal area (SA, related to social attachment behavior) are selectively activated by conditional and unconditional trust, respectively [2]. The objective of the proposed research is to automatically classify the raw signals extracted from these areas of the brain using signal processing techniques commonly applied to classify speech signals.

The data used in this research was obtained during a neuroeconomics study by Krueger *et al.* [2]. Forty-four "healthy" participants were partnered with one stranger of the same gender having a similar age and education (11 male pairs and 11 female pairs). To measure the event-related neural activity, the partners interacted with each other throughout a reciprocal Trust Game (TG) while their brains were hyperscanned in standard 3-Tesla magnetic resonance imaging (MRI) whole-body scanners. Without anonymity, the partners played 36 TGs and 16 control games (CGs) while alternating roles. Figure 5 provides a pictorial representation of the experimental setup [2, 18].

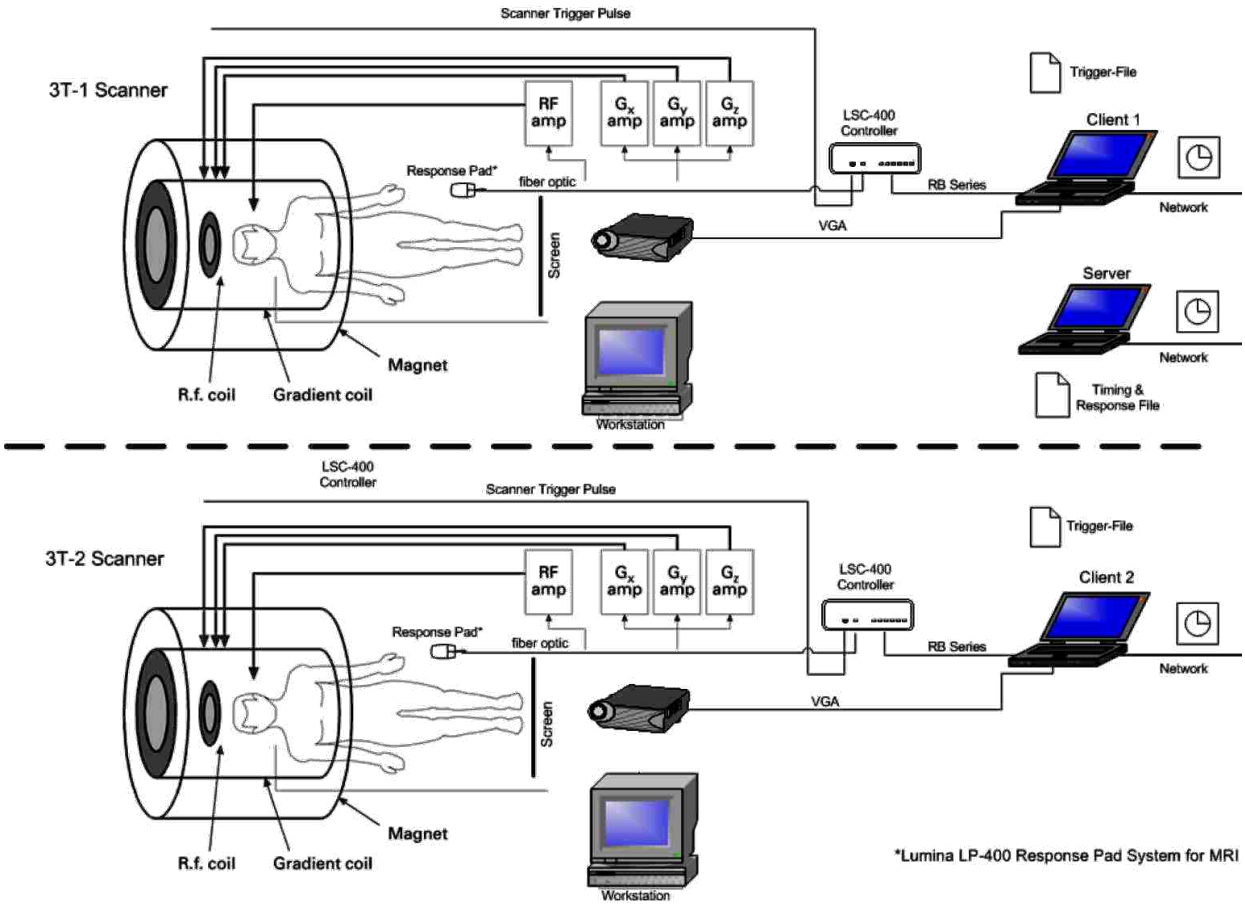

Figure 5. Reused from [2]. See permissions in Appendix B. © 2013 by the National Academy of Sciences of the United States of America. "Setup for hyperfMRI experiment. Stimuli presentation and behavioral interaction were controlled by two client computers and one server computer connected over the network. Client computers controlled the presentation of stimuli, communicating with one another through a server. The hyperfMRI experiment was started simultaneously by sending the trigger pulses from both scanners to the server, which automatically started the stimulation presentation on the clients. With a magnetically shielded LCD video projector, stimuli were back-projected onto a translucent screen. Participants viewed the screen by a mirror system attached to the head coil and made their decisions with a response pad."

The TG as applied in this study is a two-player cooperative game for financial gain at low, medium and high amounts (in cents) presented in extensive form. In extensive form, each player must make a binary decision in sequence. At the first decision node, the player who moves first (M1) must decide to either end the game, resulting in a small yet equal payoff amount for both players or send a preset amount to the player who moves second (M2) thus trusting that M2 will choose a larger payoff for both players. Then, M2 must

decide to either reciprocate M1's trust by sending a portion of the increased amount back to M1 or defect by keeping entire amount. For a depiction of this voluntary trust game, see Figure 6. In the CGs, the pairs did not interact. Each player was simply presented with the same binary decisions along the same timeline [2, 18].

Figure 6 (next page). Reused from [2] See permissions in Appendix B. © 2013 by the National Academy of Sciences of the United States of America. "Experimental design. (a) Voluntary trust game. Partners made sequential decisions as first mover (M1) and second mover (M2) for payoffs in cents [c: (cM1,cM2)] presented in a binary decision tree. M1 can choose left (nontrust) and quit the game with a small payoff for M1 and M2 (e.g., [5,5]) or can choose right (trust) to continue the game. M2 can then choose left (reciprocate), giving them both a higher payoff (e.g., [10,15]) or choose right (defect), resulting in an even larger payoff to M2 and a payoff of zero to M1 (e.g., [0,25]). Payoffs (p1–p6) were split into three types: low (p1–p2), medium (p3–p4), and high (p5–p6). (b) Time line for a single trust game. Partners were introduced by seeing each other by webcam, and digital photographs were taken to be used for game trials. A 2-s introductory screen informed partners of the role that they were playing (M1 or M2). M1 saw the game tree, had to make a decision (nontrust or trust) within 6 s, and waited 6s for M2's decision while seeing a blank screen. M2 saw a blank screen for 6 s, saw the game tree with M1's decision, and had to make a decision (reciprocate or defect) within 6 s. If M1 had chosen not to trust M2, the game was over, and M2 saw M1's decision for 6 s. Partners saw the outcome of the game for 4 s followed by a blank screen with a jittered interstimulus interval of 2–6 s."

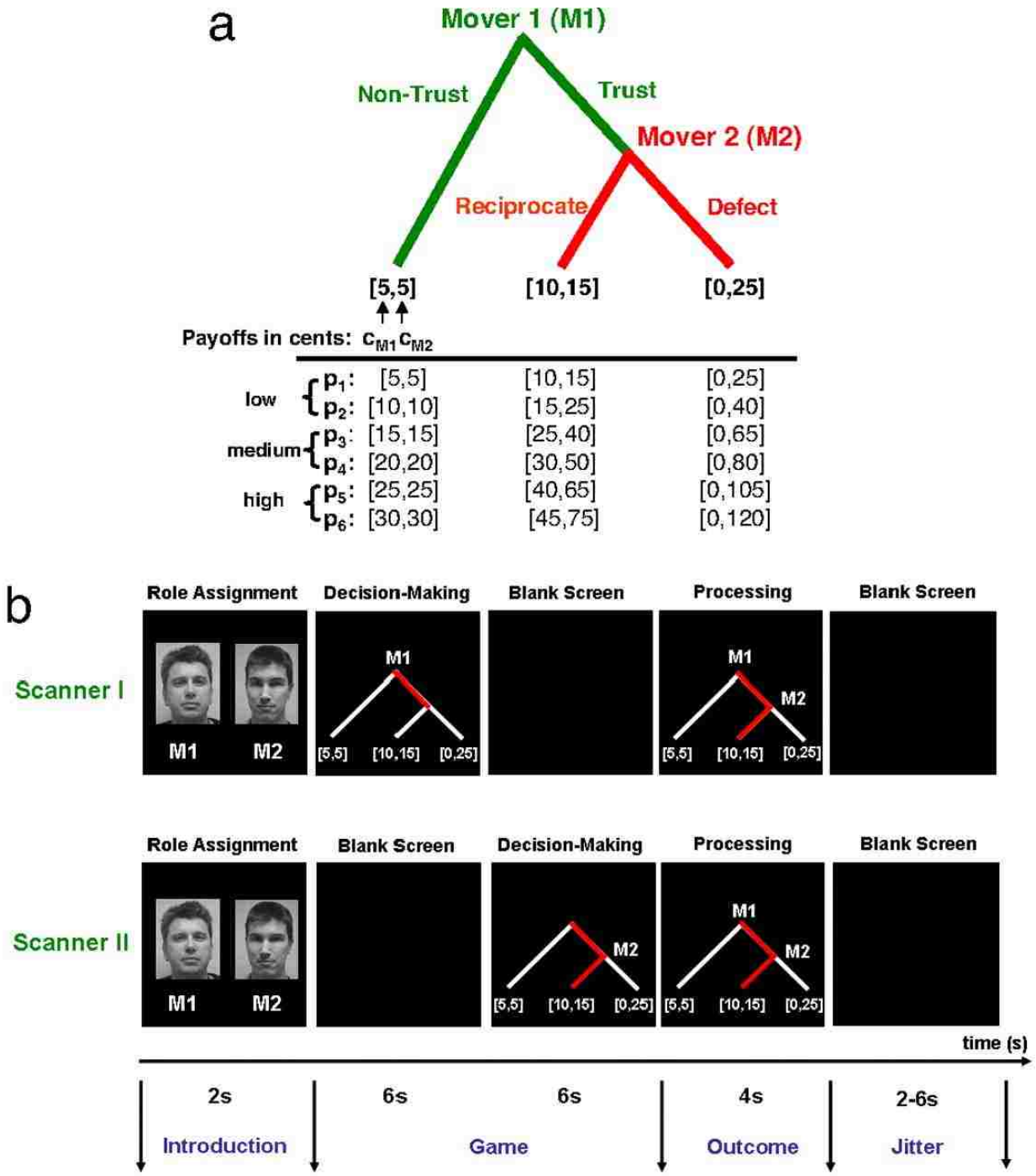

The study results reveal that the M1 decided to trust M2 eighty-four percent of the time while M2 decided to reciprocate seventy-seven percent of the time compared to seven percent defect. Moreover, these decisions were made in about 2.5 seconds on average. After the experiment, participants felt closer to and more of a partner to one another

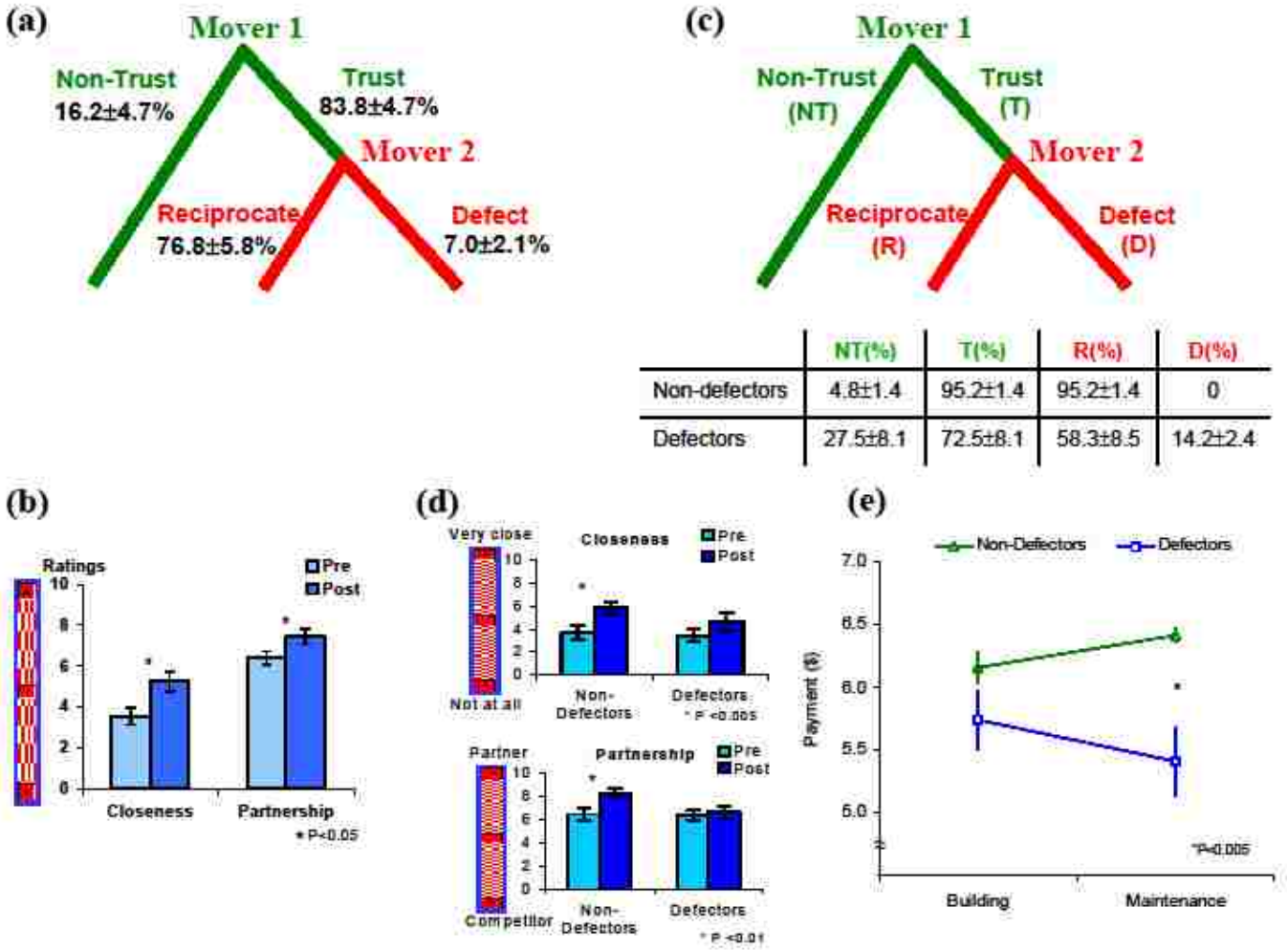

	NT(%)	T(%)	R(%)	D(%)
Non-defectors	4.8±1.4	95.2±1.4	95.2±1.4	0
Defectors	27.5±8.1	72.5±8.1	58.3±8.5	14.2±2.4

Figure 7. Reused from [2] See permissions in Appendix B. © 2013 by the National Academy of Sciences of the United States of America. "Behavioral results for decisions to trust. (a) Behavioral choices (multisubject level ±SEM). First movers decided to trust more often than not to trust, and second movers reciprocated more often than they defected (note that decisions not to trust, reciprocate, and defect add up to 100%). (b) Pre- and postexperiment ratings (multisubject level ± SEM). Before and after scanning, partners were asked to rate their closeness and partnership to one another on 11-point Likert scales. After the experiment, participants felt closer to each other and ranked themselves more as a partner to the other person. (c) Behavioral choices (group level ±SEM). Partners in the nondefector trusted more and reciprocated more compared with the defector group. (d) Pre- and postexperiment ratings (±SEM). Before and after scanning, partners were asked to rate their closeness and partnership to one another on Likert scales. Partners in the nondefector group felt closer to each other and ranked themselves as more of a partner to the other person after the experiment. (e) Earnings (group level ±SEM). The defector group earned less money than the nondefector group. Earnings decreased for the defector group but increased for the nondefector group across stages."

according to pre- and post-experiment questionnaire results. The percentiles provided

above are approximations of averages. The actual amounts with standard deviation are provided in Figure 7 [2].

During analysis, this partnership was divided into two phases: *partnership building* and *partnership maintenance*. Then, pairs of participants were further divided into groups based on whether or not M2 ever decided to defect. Remarkably, this split resulted in an equal number of pairs having comparable age ranges and education levels. The only slight imbalance was the gender distribution. The "non-defector" group, in which none of the players ever defected their partner's decision to trust, comprised 6 female pairs and 5 male pairs whereas the "defector" group, in which M2 chose to defect at times, contained 6 male pairs and 5 female pairs [2].

In the non-defector group, trust increased from the partnership building phase to the maintenance phase and was higher than the defector group overall. The decision times decreased by 20%. The pre- and post-experiment questionnaire results of closeness and stronger partnership more accurately described the non-defector group. Overall, the non-defector group earned more and these earnings increased across phases. Conversely, trust decreased from building to maintenance phases in the defector group. They trusted more often in the lower payoff games than the medium-to-high payoff games, and the decision times only decreased by 10%. In the defector group, the overall earnings decreased and they were lower than the non-defector group. A graphical summary of the trust-reciprocate history and the decision speed is illustrated in Figure 8 (see [2]).

Results from general linear model (GLM) analysis suggest that activated brain regions in the PcC is critical in trust development corresponding to assumptions made about intentions in order to anticipate behaviors. For the first movers, the PcC yielded

higher activation during different phases for each group according to these mental calculations performed about their partners. The consequences of various mental calculations were conveyed in decision times and payoffs. Specifically, for the non-defector group, PcC activation was higher during the partnership building phase while the higher activation in the PcC occurred during the partnership maintenance phase for the defector group.

In comparison, the trust-reciprocate decision related to higher activation in the SA along with the adjoining hypothalamus for the non-defector group during the building phase and the higher activation in the VTA for the defector group during the maintenance phase as shown in Figure 9. The authors of [2] attributed these behaviors to unconditional trust and conditional trust. Unconditional trust, associated with the non-defector group, presumes trustworthiness while conditional trust, associated with the defector group, presumes self-interest [2].

Because the biomedical research of Krueger et al. acquired sizeable amounts of data, which resulted in costly computation and analysis time, there is high demand for robust, model-based automatic processing [29]. In compliance with the sensing component of SSP, the objective of this research is to explore event-related hyper-fMRI obtained during non-anonymous, interchanging multi-round volunteer trust games to be used for prediction of behavior during social economic exchange [2]. Hyper-fMRI data will be the direct input for an algorithm employing advanced signal processing techniques, namely hidden Markov models (HMM) and support vector machines (SVM), to classify signals associated with the decisions to trust or not trust.

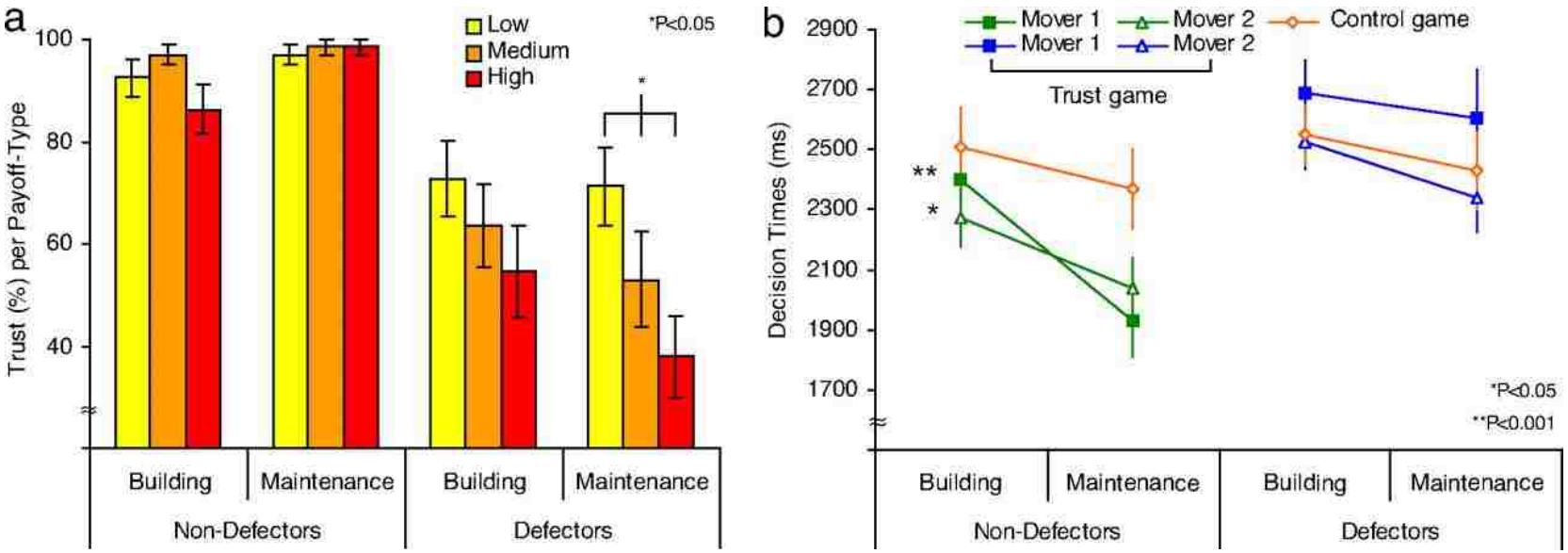

Figure 8. Reused from [2] See permissions in Appendix B. © 2013 by the National Academy of Sciences of the United States of America.. "Behavioral results for trust development. (a) Behavioral choices (±SEM). Trust in the nondefector group was higher than in the defector group and increased across stages. Trust in the defector group decreased across stages and depended on the payoff type. In the maintenance stage, trust in this group occurred more often in the low-payoff games compared with the medium- and high-payoff games and in the medium- compared with the high-payoff games. (b) Decision times (±SEM). Decision times for trust games became faster for the nondefector group across stages, and decision times accelerated by 20% for first movers and by 10% for second movers. Behavioral results for trust development."

Figure 9 (next page). Reused from [2] See permissions in Appendix B. © 2013 by the National Academy of Sciences of the United States of America. "Brain responses for trust maintenance. (a) Unconditional trust. In the nondefector group, decisions to trust contrasted with decisions to reciprocate revealed a higher activation in the SA compared with the defector group. Pairs who showed the highest trust-reciprocate history (frequency) in their decisions also showed the highest activation (parameter estimates) in the SA. (b) Conditional trust. In the defector group, decisions to trust contrasted with decisions to reciprocate revealed a higher activation in the VTA compared with the nondefector group. Pairs who showed the lowest trust-reciprocate history (frequency) in their decisions also showed the highest activation (parameter estimates) in the VTA. (c) Brain-to-brain correlation (±SEM). In the nondefector group, brain-to-brain correlations increased in the SA across stages. In the maintenance stage, partners in the nondefector group became synchronized in their SA BOLD amplitudes as first movers in adjacent trials of trust games."

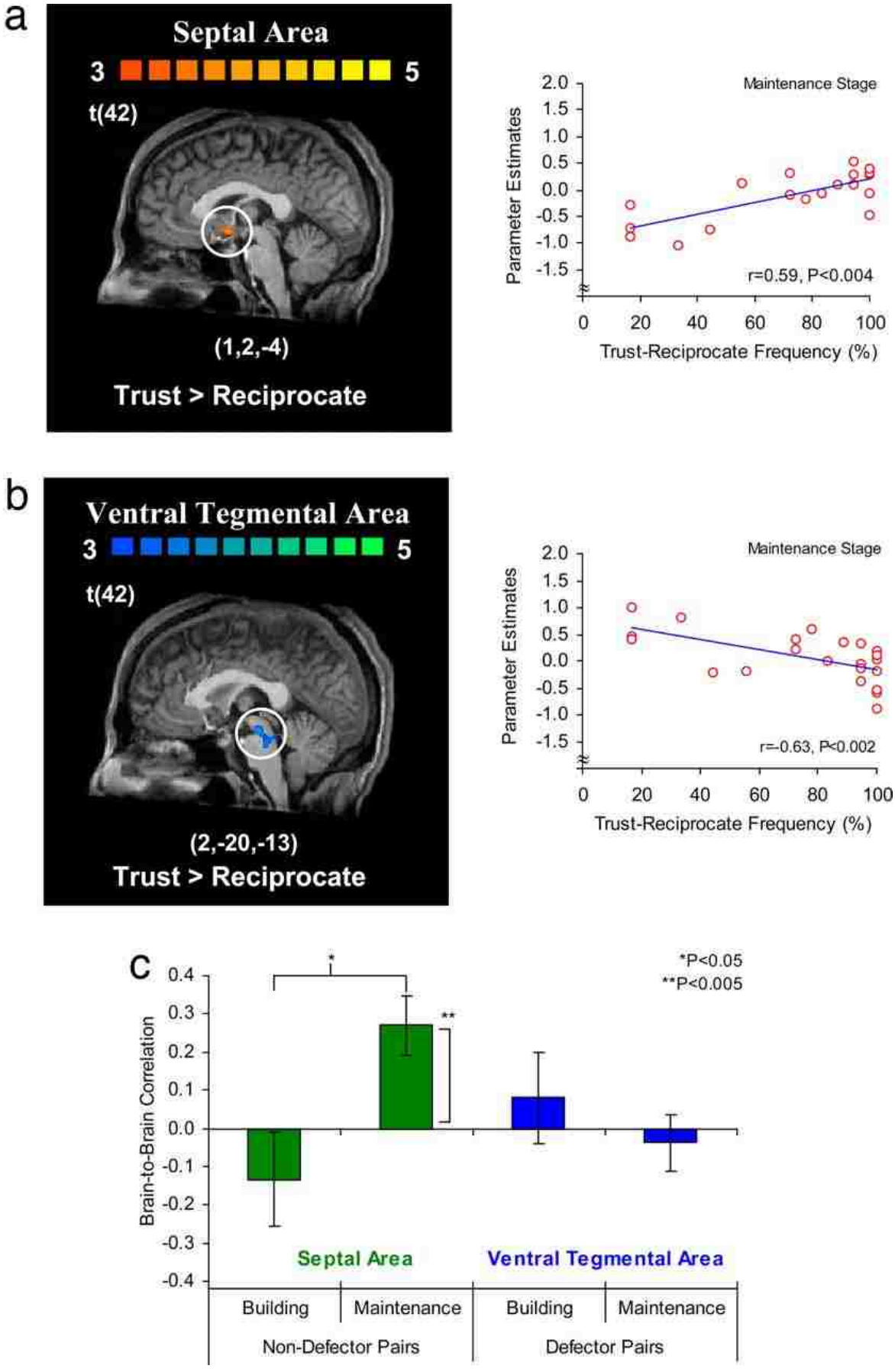
a
Septal Area
3
5
t(42)
(1,2,-4)
Trust > Reciprocate
Maintenance Stage
Parameter Estimates
r=0.59, P<0.004
Trust-Reciprocate Frequency (%)
b
Ventral Tegmental Area
3
5
t(42)
(2,-20,-13)
Trust > Reciprocate
Maintenance Stage
Parameter Estimates
r=-0.63, P<0.002
Trust-Reciprocate Frequency (%)
c
*P<0.05
**P<0.005
Brain-to-Brain Correlation
Septal Area
Ventral Tegmental Area
Building
Maintenance
Building
Maintenance
Non-Defector Pairs
Defector Pairs

3. Current Status of Knowledge

To date, two of the most popular signal processing algorithms for classification are Hidden Markov Models (HMM) and Support Vector Machines (SVM). Both schemes are embraced in a wide variety of applications, and in fact, many researchers are combining the advantages of both to form a yet more robust algorithm. [29-42]. Altun *et al.* were one of the first to hypothesize that incorporating SVM with HMM will relax the limitations of HMMs while still retaining their advantages [32]. Various applications can also be found for this type of hybrid algorithms [30-43].

3.1 Other Applications Using Hidden Markov Models

HMMs generally represent time-dependent stochastic processes and have been used broadly and effectively in speech processing [44, 45]. Cohen surveyed potential methods and applications of HMM in processing biomedical signals such as bioelectric signals (e.g. electroencephalography, EEG and electromyography, EMG), bioacoustics (e.g. phonocardiograms and ultrasonography) signals and imaging signals (e.g. magnetic resonance imaging, radiography and tomography). He proposed to use the discrete-density hidden Markov models (DD-HMMs) in which the signal samples (observations) were discrete so that they were quantized scalar or vector symbols. Cohen also proposed to use the continuous-density HMMs (CD-HMMs), which allowed continuous (not quantized) observations. Because DD-HMMs depend on a quantizer and thus by nature are inherited with quantization errors, they are not ideal. Although these disadvantages are not found in CD-HMMs (thus making CD-HMMs more accurate than DD-HMMs), the training algorithm for CD-HMMs would be more complicated and the corresponding training database must be much larger. The CD-HMMs definitely require more computational

space and time than the DD-HMMs. HMM based methods have successfully been used in automatic speech recognition for persons with cerebral palsy. DD-HMMs used in EEGs obtained from sleep studies achieved a recognition rate around 95% in patient-dependent (the models were trained with a training database taken from the same patient as the test database) experiments and a recognition accuracy of 72% in patient-independent studies. In protein sequence analysis, HMMs successfully identified conserved regions called "motifs" that may be functionally important. Cohen further mentioned the need to use HMMs for more biomedical signal processing applications as improvements are made and as more literature becomes available from similar applications. The biomedical signal processing applications are ever increasing and ideal for EEG and EMG data but quite few works have been reported for fMRI data [46].

Yong Li *et al.* applied HMM to EEG signals for classification between left and right voluntary finger movements. Recorded signals were analyzed with a leave-one-out training and testing procedure [47]. The signal classification procedure began with pre-processing of EEG signals, i.e., reference selection, reduced sampling rate, segmentation into individual trials. For independent feature extraction, HMM was applied to the enhanced series signals after filtering the multi-channel EEG in both spatial and frequency domains for each trial. Later, the authors of [47] used a perceptron neural network, a simple linear classifier, with two inputs and one output to differentiate between left or right finger movements. The average classification accuracy of 93.2% (with a standard deviation of 2.08%) is about 5 to 10% higher when the two combined independent features are used. It was concluded that the noise insensitivity and the high classification accuracy were advantageous. Based on their classification accuracy, the trial was successful for the five

healthy, right-handed male subjects used. An extension from offline to online analysis was also stated in [47].

Jin He *et al.* proposed a real-time activity classification algorithm for a wearable sensor network with accelerometers to monitor physical activity, which could be used in medical care [48]. The authors of [48] considered a three-sensor network with sensors placed at the chest and outer thighs of a subject. To reduce the data transmission rate and volume, Jin He *et al.* applied the window processing method to discern significant information. To classify whether subjects were sitting, standing, falling or transitioning between these "stable" states, they

1. used HMMs to build a framework,
2. trained the HMMs using the Baum-Welch algorithm,

   and
3. estimated most probable hidden states with the Viterbi algorithm.

Jin He *et al.* achieved an accuracy of greater than 95% in the classification of their 550 samples obtained from 5 subjects doing 11 different activity series 10 times each. Given the results, the proposed algorithm proved to be fairly successful, but the authors offered no explanation for the few errors present [48]. It appears that binary activity such as sitting or standing with single transition in between states yielded 100% accuracy. However, more complicated activity with multiple stable states and transitions slightly reduced the level of accuracy. Next, Jin He *et al.* proposed to increase the number of sensors, subjects and activities to the model. This variety will likely significantly reduce the accuracy but may allow for more robust classification of more complex activity [48].

Georgoulas *et al.* presented a method to automatically classify fetuses as normal and hypoxic based on the value of their umbilical cord pH value extracted from the fetal heart rate [49]. Fetal heart-rate recordings were obtained from the cardiotocograms acquired using scalp electrodes from 36 women during the later weeks of pregnancy. For pre-processing, "stable" segments, as defined by the relatively small difference in beats per minute in adjacent segments, of the signal were identified. Using the segmental k-means training algorithm, the two HMMs estimated the two different situations (normal and hypoxic). To evaluate the performance of the classification, the authors of [49] applied the multifold cross-validation technique. The average overall classification rate was more than 81% with the number of hidden states varying from 3 to 8. The maximum classification rate was 90% for the normal case using 6 hidden states and 88% for the abnormal (hypoxic) case using either 5 or 8 hidden states. The most balanced classification performance occurred using 3 or 7 hidden states but varied greatly using other numbers of hidden states. Georgoulas *et al.* concluded that there can be pre-set criteria to distinguish normal from abnormal cases successfully. Next, they proposed the use of additional index components for more objective classification [49].

Shimokawa *et al.* aimed to predict human investment behavior using functional near-infrared spectroscopy (fNIRS) to measure changes in cerebral blood flow and thus brain activation [50, 51]. Subjects' brains were scanned using fNIRS as they participated in single-subject sequential investment task (SIT). For a predictive model, they used a three-layered perceptron to depict the complex relationship between these changes in cerebral blood flow and the investment behavior. To increase the robustness of estimation precision, they further employed the Bayesian estimator involving parameters and hyperparameters

using the Markov chain Monte Carlo (MCMC) algorithm. They also applied a moving-average smoother to remove noise from the investment-rate time-series data. Using their method, one could predict the investment rate with relatively high precision. For most periods, the real investment rate fell within the 50% prediction interval. Based on the mean-squared deviation results with and without blood flow data, the authors of [50, 51] achieved a 59.8% improvement by adding blood flow data to the investment rate from the previous period. Shimokawa *et al.* suggested a need for additional experiments to reach conclusions. They acknowledged that although fNIRS is less restrictive and more economical than fMRI, it has low spatial resolution and shallow observation capability resulting in "limited range of analysis and precision". They suggested to combine the strengths of both fMRI and fNIRS for brain-computer interfaces [50, 51].

3.2 Other Applications Using Support Vector Machines

Support Vector Machines (SVMs) have recently grown in popularity for pattern recognition and classification applications in neuroscience and medicine. They could lead to high classification accuracy but are constrained by the number of classes, kernel selection and method [29, 52-57]. Many more applications, however, rely on hybrid methods as opposed to a standalone SVM [29-42].

De Martino *et al.* explored a generalized approach to fMRI independent component analysis and classification [52]. In contrast to univariate statistical analyses, spatial maps were found by the intrinsic structure of the data instead of the identification of *a priori* region of interest. This blind, data-driven approach allows for the feature extraction from the whole brain to avoid missing any pertinent information that might be found outside of the regions of interest. The researchers are able to explore the significant spatiotemporal

patterns such as “networks of functionally connected brain regions and structured artifacts” at any location and advance beyond the insignificant portions, thus, obtaining a more meaningful subset of the components [52].

Taking advantage of the benefits of each, De Martino *et al.* incorporated an SVM with univariate and multivariate feature selection strategies to discriminate patterns in fMRI. Using an iterative, data-driven computer procedure, their method offered blind detection of patterns in the spatio-temporal domain and hence reduced the need for *a priori* information about dimensions and locations. Their approach, further reduced the need for whole-brain analyses and was more sensitive to these discriminative patterns. They also recursively eliminated least discriminative patterns [53] [55].

Mahmoud and Olatunji proposed a method for training and testing handwritten Arabic numbers using combinations of multi-span features [43]. They identified the combinations that presented the best classification rates for SVM and compared them to the published results of HMM and Nearest Mean (NM) classifiers. The authors of [43] extracted the angular, ring, horizontal, and vertical span features and concluded that the angular and horizontal span features achieved the highest recognition rates when compared to other combinations. The average classification rates for SVM, HMM, and NM were 99.4%, 97.99%, and 94.35%, respectively. The authors would like to their work using statistical and syntactical features [43].

Tsochantaridis *et al.* proposed a generalized multiclass SVM learning algorithm for supervised learning, which extracted features from both inputs *and* outputs [58]. The authors took advantage of sparseness and structural decomposition with a cutting plane algorithm and applied their method to several different types of classification problems

including classification with taxonomies, label sequence learning, sequence alignment, and natural language parsing[58].

For classification with taxonomies, they indexed title and claim tags from an International Patent Classification (IPC) scheme and subsampled the training data to study the effects of the size of the training set [58]. For this dataset, they found that the hierarchical SVM learning algorithm had a higher training accuracy and a lower tree loss than the standard multiclass SVM. For label sequence learning, HMM, CRF and perceptrons led to a higher error rate than that of SVM. In sequence alignment, SVM had a better performance than the generative model with a lower number of training sets but comparable with a larger number of training data sets. Finally, the authors compared different forms of SVM to the generative PCFG model in natural language parsing with context-free grammar from which they concluded that all of the models performed comparably with less CPU time used by the generative PCFG model [58].

Boyle *et al.* evaluated the performance of SVMs for the classification of medical tasks. The researchers used SVM to diagnose certain conditions within the Breast Cancer, Parkinson and urological databases. As with all signals, the information from the databases had to be preprocessed by normalization and missing treatment data. Then, the datasets were supplied to the SVM to determine whether there was a condition or not. Although the data preprocessing costs more time, the benefit is a 15% increase in the system accuracy. Missing treatment is more common for the urological database than for the Breast Cancer and Parkinson databases. Therefore, preprocessing is needed for less refined datasets [57].

In classifying whether or not a condition existed, the correct classification rates for Breast Cancer, Parkinson and urological databases were 97.89%, 91.79% and 84.25%.

However, the authors of [57] claimed that the lower precision did not always reflect the truth because of the skewed distribution of the output classes, which was the reason for the high need of the preprocessing to build an even distribution. Because of the high correct classification rates, Boyle *et al.* proposed to use their technique to classify more common conditions by adding multiple classes [57].

4. Our Approach

4.1 Feature Extraction for fMRI in Psychological Study

For the raw fMRI data, the intensity values over time (times series) of the functional data are extracted as a four-dimensional array representing each voxel location (x, y, z) and time course in a VTC file (generated by BrainVoyager QX © 2010 Brain Innovation). Additional information including resolution, space and directional conventions, directional start and end values, version number, data type, number of volumes and other header information are momentarily disregarded for the scope of this research [59, 60]. Further extracted from this four-dimensional array are time series at very specific locations. Based on previous studies [61-63], *a priori* regions of interest (ROIs) were pre-defined and

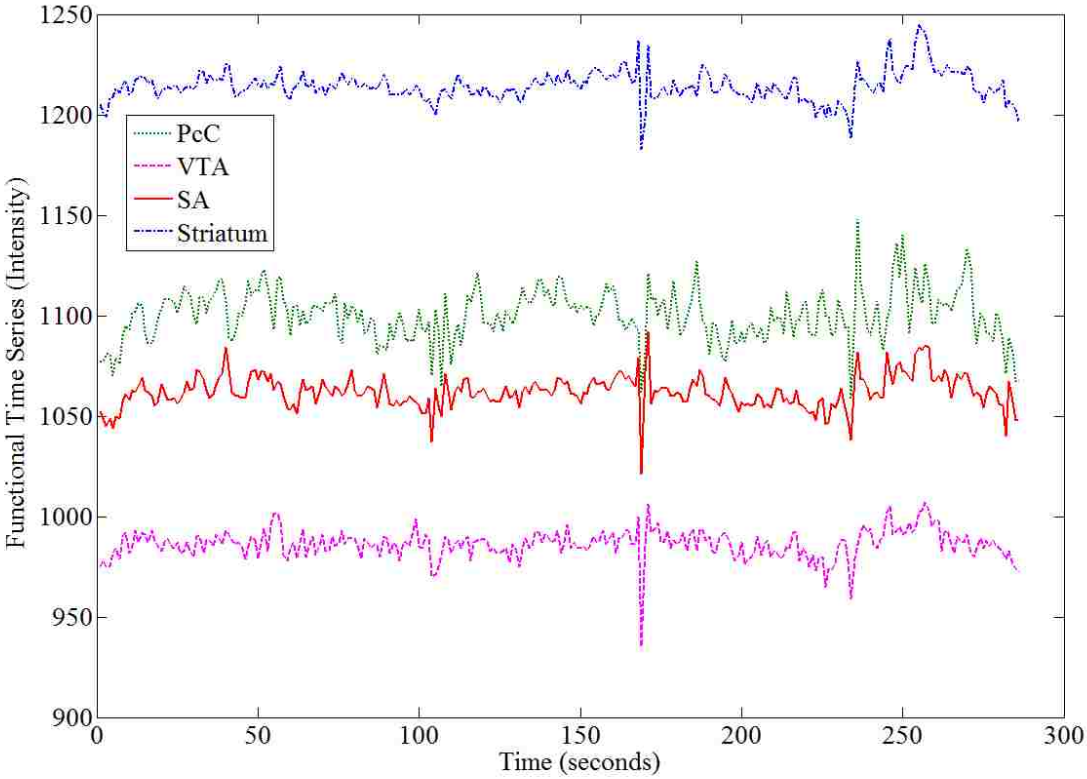

Figure 10. Full functional timecourses for Subject 15, Run 3 (maintenance phase) extracted from four Talaraich regions of interest: Paracingulate Cortex (PcC), Ventral Tegmental Area (VTA), Septal Area (SA) and Striatum.

analyzed for the voluntary reciprocal trust experiment. These regions include paracingulate cortex (PcC), septal area (SA), ventral tegmental area (VTA) and striatum. Within each ROI's activated clusters, the most significant voxel was used to define Talairach coordinates of (1, 46, 20), (6, 11, 4), (0, -10, -10) and (17, 4, 11), respectively [2]. A sample of a time series for one subject is shown in Figure 10.

For visual reference, a graphical representation of the game sequence mentioned in Section 0 is shown in Figure 11. Each pair of players played 36 reciprocal trust games and 16 control games with the latter CGs unreported. Because these games were sequential in

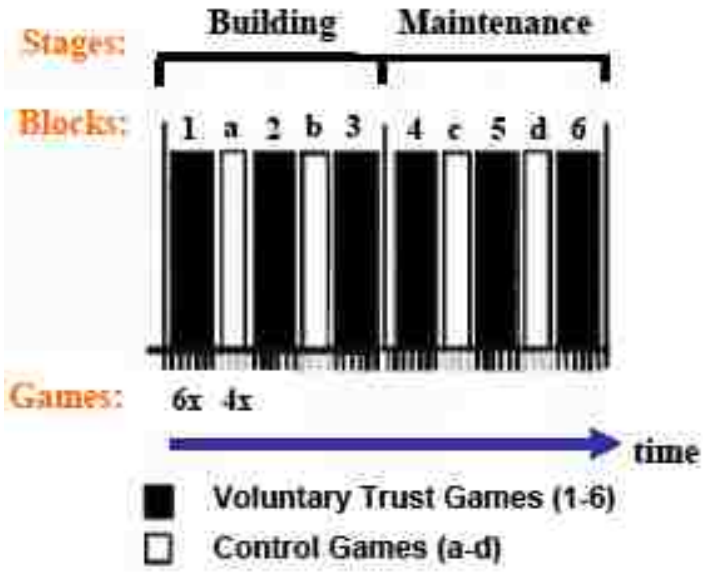

Figure 11. Reused from [2]. © 2013 by the National Academy of Sciences of the United States of America. Arrangement of games during the experiment. The experiment was split into two stages (building and maintenance), each including 18 VTGs and 8 CGs. Each stage lasted ≈12 minutes and consisted of three blocks of voluntary trust games (six games per block) and two blocks of control games (four games per block).

that each player alternated as the first mover, data for only 18 games was analyzed for each player, which were further divided into two phases (or *runs*): trust building and trust maintenance. Thus, corresponding information about each subject number, run number, game outcome (decision to trust or not trust) and game timing for 9 games was matched with times series information for each of the four ROIs. According to the game design, the

first mover's decision was made in the 6 seconds following a 2 second introductory screen. Therefore, if the game timing for any subject *s* at run *r* be t_{sr}, then the relevant time series

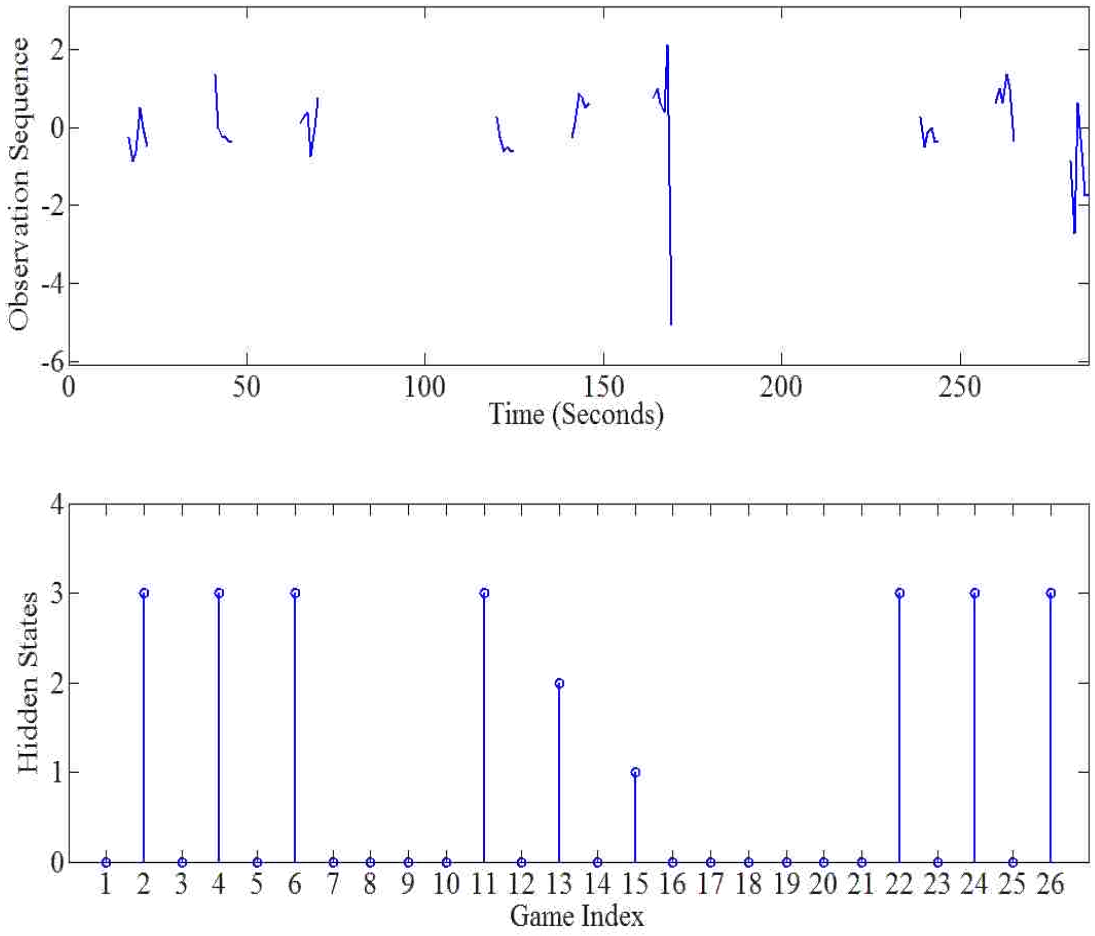

Figure 12. (Top) Observation Sequence: Intensities from a functional time course during the 6-second decision period extracted from a full timecourse of Septal Area of Subject 15, Run 3. (Bottom) Hidden States: Corresponding outcomes (decisions) at each decision period, i.e., 1 for trust-defect, 2 for trust-reciprocate and 3 for not trust.

can be extracted from $t_{sr} + 3$ to $t_{sr} + 8$ as shown in Figure 12. In this dissertation, these fMRI data will be automatically classified into two groups (trust or non-trust) according to game outcomes. In the next sections, advanced classification techniques, namely linear classifier, support vector machine and hidden Markov model, will be investigated to establish a robust scheme on this matter.

4.2 Classification Using Linear Classifier

In *linear classification*, the aim is to divide a set of features into two classes that the data is linearly separable. A linear classifier mathematically separates data with a line based on features extracted from each data point. Given a set of training data, each point (*x*, *y*) can be classified by the response $l = sign(ax + by + c)$, where *a*, *b* and *c* are constants that define a line. Thus, each point is projected onto a line as in Figure 13, and the sign, positive or negative, of each point indicates its classification. To determine the equation of this discriminant line, solve *ax* + *by* + *c* = 0. Training data is used to optimize the parameters of the line.

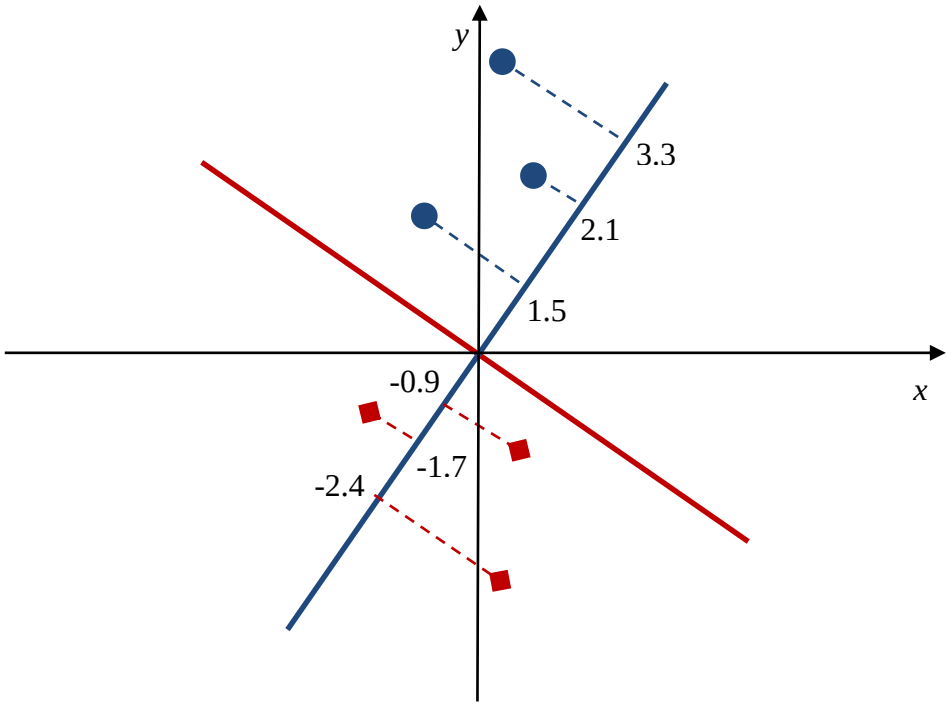

Figure 13. Illustration of points projected onto a line for linear classification.

To transform the response into a probability of correct classification, use the *logistic function* such that

$$P[l = \pm 1|x] = \frac{1}{1 + \exp(\mp(ax + by + c))} \quad (1)$$

where *l* can take values +1 or -1. Given any set of line constants, the likelihood of a correct classification, i.e. the probability of correctly classifying each item in the training set is given by

$$\prod_{i}^{N} P[l_i|x_i] = \prod_{i}^{N} \frac{1}{1 + \exp(-l_i(ax_i + by_i + c))}. \quad (2)$$

Then, the goal is to find the line parameters that minimize the *loss* (or *cost*) *function* in Equation 3 (or maximize Equation 2) by finding $-\nabla L$, where

$$L = \sum_{i=1}^{N} \log\left(1 + \exp\left(-l_i(ax_i + by_i + c)\right)\right). \quad (3)$$

4.3 Classification Using Support Vector Machines (SVMs)

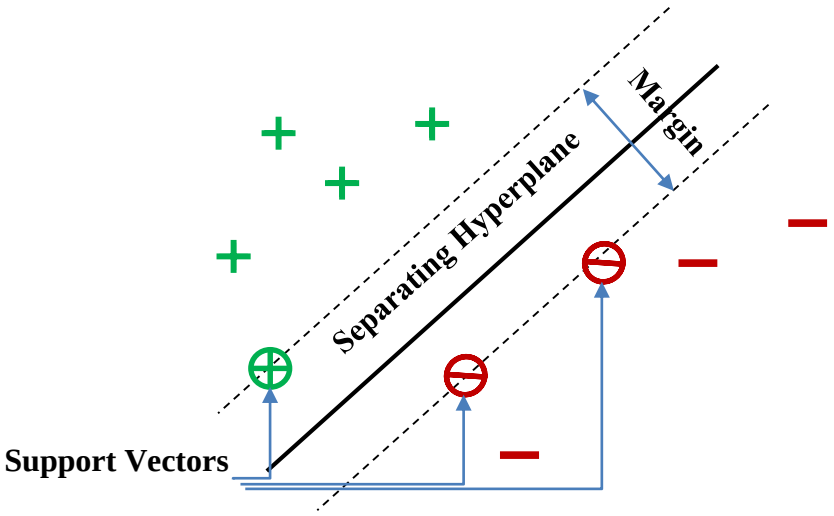

Figure 14. Illustration of basic support vector machine for separable data.

Support Vector Machine (SVM) is a particular classifier using *sparse* training samples, (x_i, y_i), where x_i is a set of points (vectors) and y_i constitutes the corresponding class assignments. Its complexity is expressed by the classification data set. Because

kernel-based transformations allow for computation of the dot product in higher dimensions, d , SVMs apply kernel-based transformations as in Equation (4) for optimization on the input dataset where $x_i \in \mathbb{R}^d$, where

$$K(x_i, y_i) = \langle \Phi(x_i), \Phi(x_j) \rangle \tag{4}$$

and $y_i = \pm 1$. The form of the kernel-based decision function is expressed by

$$f(x) = \sum_{i=1}^{N} \alpha_i y_i K(x, y_i) + b \tag{5}$$

Two of the common kernel functions, *polynomial* and *radial basis*, are described by

$$K(x_i, y_i) = (\langle x_i, y_i \rangle + 1)^d \quad \text{(polynomial)}, \tag{6}$$

$$K(x_i, y_i) = \exp\{-\Psi(|x_i - y_i|^2)\} \quad \text{(radial basis)}, \tag{7}$$

respectively. Although they are highly data-dependent and the corresponding convergence is slower, radial basis functions (RBFs) have better performance. By definition, the classification task scales linearly with the number of support vectors, N [29]. Suppose x is the d-dimensional coordinate. The *hyperplane* for a SVM is characterized by

$$\langle w, x \rangle + b = 0, \tag{8}$$

where w is the "*weight vector*". The additional constraint on w should also be imposed such that

$$y_i(\langle w, x_i \rangle + b) \geq 1. \tag{9}$$

Like a linear classifier, an SVM classifies data by finding a d-dimensional hyperplane as described by Equation (8) with the largest margin between two classes to separate the data points from each class into different groups as shown in Figure 14. If the data is separable, all data points will lie on either side of the hyperplane as described by Equation (9) where the support vectors are those data points x_i that lie on the boundary for which $y_i(\langle w, x_i \rangle + b) = 1$. Equation (10) provides the optimal SVM classification solution:

$$\text{class}(z) = \text{sign}(\langle w, x \rangle + b). \quad (10)$$

However, a soft-margin hyperplane is necessary if the data is non-separable, which is actually the case with the fMRI data in this study.

For non-separable data, several algorithms are common for optimizing the aforementioned hyperplane. In this study, the standard *Sequential Minimum Optimization* (SMO), *Least-Square* (LS) and *Quadratic Programming* (QP) methods were explored where SMO algorithm minimizes the L^1-norm and the latter two methods minimize the L^2-norm with added *slack variables* s_i and a *penalty parameter C*. To solve the L^1-norm minimization problem, one needs to carry out

$$\min_{w,b,s} \left(\frac{1}{2} \langle w, w \rangle + C \sum_i s_i \right), \quad (11)$$

subject to

$$y_i(\langle w, x_i \rangle + b) \geq 1 - s_i, \quad (12)$$

$$s_i \geq 0.$$

To solve the L^2-norm minimization problem, one has to undertake

$$\min_{w,b,s} \left(\frac{1}{2} \langle w, w \rangle + C \sum_i {s_i}^2 \right), \quad (13)$$

subject to the same constraints given by Equation (12). It is apparent that adjusting *C* up or down will change the sensitivity to the slack variables so misclassification becomes more or less important, respectively [64-66]. In this research, the kernel and algorithm were chosen according to the preliminary classification results depicted in Figure 15.

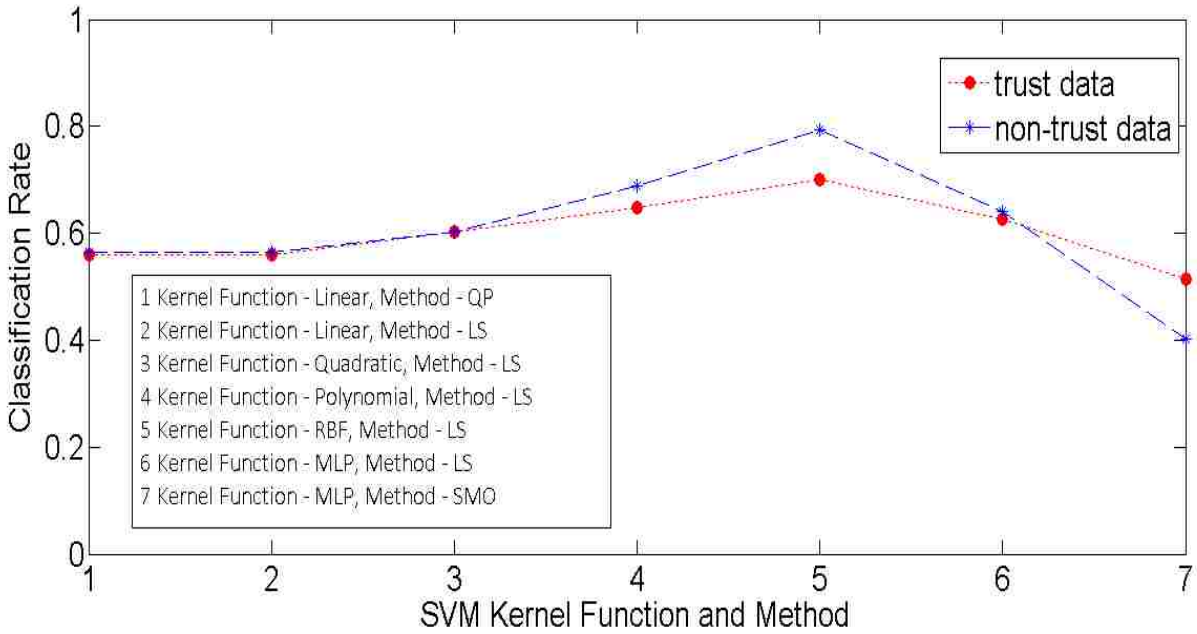

Figure 15. Classification rates for various kernel methods (linear, quadratic, polynomial, RBF, and MLP) and various methods (QP, LS, and SMO). Note that "quadratic" means a quadratic polynomial kernel, "polynomial" means a third-degree polynomial kernel, and MLP means "multilayer perceptron".

4.4 Classification Using Hidden Markov Models (HMMs)

To facilitate our analysis, the theory of HMM (see [44]) is briefly introduced here. First, we define the following parameters according to [67]. Based on a player's reaction, the outcomes of this game can be grouped into three sets, namely Non-Trust (NT), Trust-Defect (TD) and Trust-Reciprocate (TR). Since we only analyze the data from the first player/mover in Figure 7, the outcomes labeled as TD and TR represent *trust*, while the outcomes labeled as NT represent *non-trust*. We use the abridged notation *trust Septal*, *trust Ventral*, *non-trust Septal* and *non-trust Ventral* to specify the data acquired from different brain regions for different classes of outcomes. The first word indicates the type of outcome, namely trust or non-trust while the second word indicates the brain region, namely "Septal" for septal area and "Ventral" for ventral tegmental area. The HMMs for this fMRI application are established as follows.

1. $\tau_O \stackrel{\text{def}}{=} \{1, 2, \ldots, T\}$, where T is the sample size. τ_O is the set of observing times (sampling time indices) for acquiring the fMRI time series.
2. $\tilde{O} \stackrel{\text{def}}{=} [\vec{o}_1 \quad \vec{o}_2 \cdots \vec{o}_T]$ denotes the set of fMRI observations corresponding to τ_O, where

$$\vec{o}_m \stackrel{\text{def}}{=} [s_m, v_m]^T,\ 1 \leq m \leq T; \tag{14}$$

s_m and v_m are the observations acquired from the septal area and the ventral tegmental area at time m, respectively. We cluster the two-dimensional fMRI observations $\tilde{O}$ into ℵ groups using K-means method (see [68]). Then, we establish a new data matrix

$$\tilde{Q} \stackrel{\text{def}}{=} [\vec{q}_1 \quad \vec{q}_2 \cdots \vec{q}_T] \tag{15}$$

where $\vec{q}_m \stackrel{\text{def}}{=} [\bar{s}_m, \bar{v}_m]^T$ such that $[\bar{s}_m, \bar{v}_m]^T$ denotes the cluster mean vector to which $[s_m, v_m]^T$ is closest.

3. $\tau_E \stackrel{\text{def}}{=} \{t_1, t_2, \ldots, t_L = T\}$ denotes the *event detection time*, where $t_1 < t_2 < \cdots < t_L$, $\tau_E \subset \tau_O$. An event detection means that the first player decides to trust or distrust the second player in the game. L is the total number of event detections.
4. $E \stackrel{\text{def}}{=} \{e_1, e_2, \ldots, e_L\}$ is the sequence of the L detected events corresponding to τ_E, where $e_k, 0 \leq k \leq L$ can be either "trust" or "non-trust". Therefore, the clustered fMRI time series $\vec{q}_{t_l}, \vec{q}_{t_l+1}, \ldots, \vec{q}_{t_{l+1}}$ with respect to detection events e_{l+1} can be classified into either trust or non-trust, where $(t_l, t_{l+1}) \subset \tau_E$, for $0 \leq l \leq L - 1$.
5. $S \stackrel{\text{def}}{=} \{\xi_1, \xi_2, \ldots, \xi_N\}$ represents the state space of HMMs, where N is the number of states.
6. The HMM is denoted by

$$\gamma \stackrel{\text{def}}{=} (\Pi, \tilde{A}, \tilde{B}), \tag{16}$$

where the initial state distribution is given by

$$\Pi \triangleq \{\pi_1, \pi_2, \dots, \pi_N\} \tag{17}$$

and the state transition probability matrix is $\tilde{A} \in \mathcal{R}^{N\times N}$. The (p, q)-entry in $\tilde{A}$ is

$$a_{pq} \triangleq p(\xi_q|\xi_p) \tag{18}$$

where $p(\xi_q|\xi_p)$ denotes the transition probability from state ξ_p to state ξ_q. $\tilde{B} \in R^{N\times\aleph}$ is the emission matrix. The (p, q)-entry in $\tilde{B}$ is

$$b_{pq} \triangleq p(\hat{o}_q|\xi_p) \tag{19}$$

where $p(\hat{o}_q|\xi_p)$ denotes the emission probability from state ξ_p to output $\hat{o}_q$. Note that $\hat{o}_q$ indicates any entry in a cluster mean vector, such as $\bar{s}_m$ or $\bar{v}_m$.

Given the clustered fMRI observations $\tilde{Q}$, the detected events E, and the initial state distributions Π, the procedure of data analysis can be illustrated by Figure 16, as follows.

Step 1: Classify the clustered fMRI time series, $\vec{q}_{t_l}, \vec{q}_{t_l+1}, \dots, \vec{q}_{t_{l+1}}$, for $(t_l, t_{l+1}) \subset \tau_E$, into *trust group*

$$\wedge \triangleq \{\vec{q}^{\,I}{}_{t_l}, \vec{q}^{\,I}{}_{t_l+1}, \dots, \vec{q}^{\,I}{}_{t_{l+1}}\} \tag{20}$$

or *non-trust group*

$$\vee \triangleq \{\vec{q}^{\,II}{}_{t_l}, \vec{q}^{\,II}{}_{t_l+1}, \dots, \vec{q}^{\,II}{}_{t_{l+1}}\} \tag{21}$$

according to $e_{l+1}, l = 0, 1, \dots, L-1$, where

$$\vec{q}^{\,I}{}_{t_l} \triangleq [\bar{s}^{I}{}_{t_l}, \bar{v}^{I}{}_{t_l}]^T,$$

$$\vec{q}^{\,II}{}_{t_l} \triangleq [\bar{s}^{II}{}_{t_l}, \bar{v}^{II}{}_{t_l}]^T. \tag{22}$$

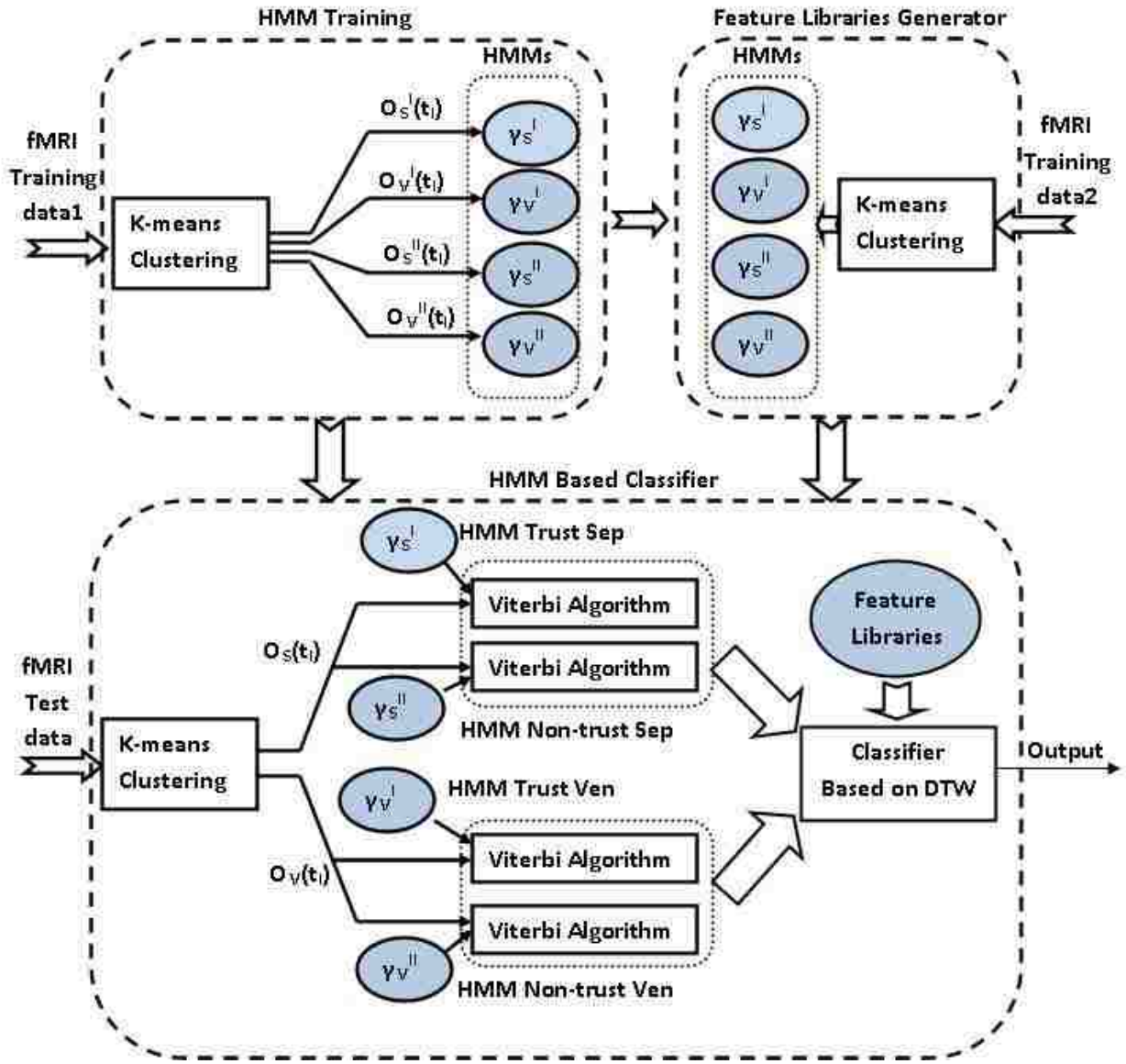

Figure 16. Block diagram of the proposed fMRI data analysis scheme. Three major components of this scheme, namely HMM training mechanism, feature library generator, and HMM based classifier, are all illustrated. Note that, "Sep" stands for the septal area, while "Ven" stands for the ventral tegmental area. fMRI training data1 and fMRI training data2 are randomly chosen among the three subset groups $\boldsymbol{\mathcal{D}_I}$, $\boldsymbol{\mathcal{D}_{II}}$ and $\boldsymbol{\mathcal{D}_{III}}$.

Step 2: Randomly divide Λ and V into training data set one, training data set two (equally extracted from Λ and V), and the test data set, where these three data sets are mutually exclusive.

Step 3: Select the state number N and the cluster number ℵ and train HMMs, namely

the HMM for trust Septal (γ_s^I),

the HMM for trust Ventral (γ_v^I),

the HMM for non-trust Septal (γ_s^{II}),

the HMM for non-trust Ventral (γ_v^I),

using training data set one. For example, γ_s^I is trained by the data sequence $\bar{s}^I{}_{t_l}, \bar{s}^I{}_{t_l+1}, \dots, \bar{s}^I{}_{t_{l+1}}, (t_l, t_{l+1}) \subset \tau_E$, for $l = 0, 1, \dots, L-1$.

Step 4: By employing the obtained HMMs in **Step 3**, establish the *feature library* based on training data set two. The feature library consists of the state sequences for the above-mentioned four classes of data. For details regarding state sequences, refer to Section 4.4.2.

Step 5: Test the HMMs obtained from **Step 3** using the test data. Employ Viterbi algorithm (see [69]) to find the optimal *hidden state sequences*. Then, the optimal hidden state sequences are compared with the feature library obtained from **Step 4** and then classified into trust or non-trust categories by invoking *dynamic time-warping (DTW) algorithm* [65].

4.4.1 HMMs Training

To make the training of HMMs converge fast with satisfactory results, proper initialization of the HMMs' parameters using the training data is necessary before the actual training process starts. The most common method for initializing an HMM model is setting $(\Pi, \tilde{A}, \tilde{B})$ randomly. Usually, random initialization is computationally-efficient. However, since the convergence speed of the training process highly depends on the initial

generator seed, which facilitates the initial point on the likelihood surface, random initialization could not always guarantee convergence. Because our focused problem is not necessary to be on-line (it cannot be on-line in practice), the *equal-occupancy state method* [70] can be employed here. The occupancy of state ν is computed and used as the stop criterion in this scheme, which is

$$\nu \triangleq^{\text{def}} \frac{\max_{\iota} \epsilon_{\iota}}{\min_{\iota} \epsilon_{\iota}}, 1 \leq \iota \leq N \tag{23}$$

where ϵ_{ι} is the number of times (occupancy) each state ι is visited using the Viterbi algorithm over all training data. In the initialization process, different initial generator seeds are employed and the one which minimizes ν defined by Equation (23) is actually selected finally.

Then, the four hidden Markov models here are trained independently using *Baum-Welch expectation maximization algorithm* [65]. To train these four models, one hundred detection events for each model, namely the HMM γ_s^I for the trust Septal data, the HMM γ_v^I for the trust Ventral data, the HMM γ_s^{II} for the non-trust Septal data, and the HMM γ_v^{II} for the non-trust Ventral data, are randomly selected from the experiments. The corresponding clustered fMRI time series (training data set one $\tilde{Q}$) are used as training data for each HMM. The auxiliary functions (see [44]) employed in the training process shown in Figure 16 are given by

$$\begin{aligned}
\Upsilon(\gamma_s^I, \hat{\gamma}_s^I) &\triangleq^{\text{def}} \sum_{\wp_s^I(t_l)} \{\mathrm{P}(\wp_s^I(t_l)|\mathrm{O}_s^I(t_l), \gamma_s^I) \times \log[\mathrm{P}(\mathrm{O}_s^I(t_l), \wp_s^I(t_l)|\hat{\gamma}_s^I)]\}, \\
\Upsilon(\gamma_s^{II}, \hat{\gamma}_s^{II}) &\triangleq^{\text{def}} \sum_{\wp_s^{II}(t_l)} \{\mathrm{P}(\wp_s^{II}(t_l)|\mathrm{O}_s^{II}(t_l), \gamma_s^{II}) \times \log[\mathrm{P}(\mathrm{O}_s^{II}(t_l), \wp_s^{II}(t_l)|\hat{\gamma}_s^{II})]\}, \\
\Upsilon(\gamma_v^I, \hat{\gamma}_v^I) &\triangleq^{\text{def}} \sum_{\wp_v^I(t_l)} \{\mathrm{P}(\wp_v^I(t_l)|\mathrm{O}_v^I(t_l), \gamma_v^I) \times \log[\mathrm{P}(\mathrm{O}_v^I(t_l), \wp_v^I(t_l)|\hat{\gamma}_v^I)]\}, \\
\Upsilon(\gamma_v^{II}, \hat{\gamma}_v^{II}) &\triangleq^{\text{def}} \sum_{\wp_v^{II}(t_l)} \{\mathrm{P}(\wp_v^{II}(t_l)|\mathrm{O}_v^{II}(t_l), \gamma_v^{II}) \times \log[\mathrm{P}(\mathrm{O}_v^{II}(t_l), \wp_v^{II}(t_l)|\hat{\gamma}_v^{II})]\},
\end{aligned} \tag{24}$$

where

$$\mathrm{O}_s^I(t_l) \stackrel{\text{def}}{=} \left[\bar{s}^I{}_{t_l}, \bar{s}^I{}_{t_l+1}, \ldots, \bar{s}^I{}_{t_{l+1}}\right],$$

$$\mathrm{O}_s^{II}(t_l) \stackrel{\text{def}}{=} \left[\bar{s}^{II}{}_{t_l}, \bar{s}^{II}{}_{t_l+1}, \ldots, \bar{s}^{II}{}_{t_{l+1}}\right],$$

$$\mathrm{O}_v^I(t_l) \stackrel{\text{def}}{=} \left[\bar{v}^I{}_{t_l}, \bar{v}^I{}_{t_l+1}, \ldots, \bar{v}^I{}_{t_{l+1}}\right],$$

$$\mathrm{O}_v^{II}(t_l) \stackrel{\text{def}}{=} \left[\bar{v}^{II}{}_{t_l}, \bar{v}^{II}{}_{t_l+1}, \ldots, \bar{v}^{II}{}_{t_{l+1}}\right]. \quad (25)$$

Moreover, $\wp_s^I(t_l)$, $\wp_s^{II}(t_l)$, $\wp_v^I(t_l)$ and $\wp_v^{II}(t_l)$ represent the state sequences corresponding to the aforementioned observations and HMMs. The corresponding *a posteriori* and *a priori* probabilities are specified as

$$\mathrm{P}(\wp_s^I(t_l)|\mathrm{O}_s^I(t_l), \gamma_s^I),$$

$$\mathrm{P}(\wp_s^{II}(t_l)|\mathrm{O}_s^{II}(t_l), \gamma_s^{II}),$$

$$\mathrm{P}(\wp_v^I(t_l)|\mathrm{O}_v^I(t_l), \gamma_v^I),$$

$$\mathrm{P}(\wp_v^{II}(t_l)|\mathrm{O}_v^{II}(t_l), \gamma_v^{II}),$$

and

$$\mathrm{P}(\mathrm{O}_s^I(t_l), \wp_s^I(t_l)|\hat{\gamma}_s^I),$$

$$\mathrm{P}(\mathrm{O}_s^{II}(t_l), \wp_s^{II}(t_l)|\hat{\gamma}_s^{II}),$$

$$\mathrm{P}(\mathrm{O}_v^I(t_l), \wp_v^I(t_l)|\hat{\gamma}_v^I),$$

$$\mathrm{P}(\mathrm{O}_v^{II}(t_l), \wp_v^{II}(t_l)|\hat{\gamma}_v^{II}). \quad (26)$$

Note that $\gamma_s^I, \gamma_s^{II}, \gamma_v^I, \gamma_v^{II}$ specify the current parameter sets for the four HMMs, while $\hat{\gamma}_s^I$, $\hat{\gamma}_s^{II}, \hat{\gamma}_v^I, \hat{\gamma}_v^{II}$ indicate the re-estimated parameters. By maximizing the auxiliary functions in Equation (24), the optimal parameter sets of the four HMMs can be obtained.

4.4.2 Feature Library Generating

Four feature libraries need to be generated. One hundred clustered fMRI time series (training data set two $\tilde{Q}$), namely $\vec{q}_{t_l}, \vec{q}_{t_l+1}, \ldots, \vec{q}_{t_{l+1}}, t_l \in \tau_E$ are randomly selected from

Λ and $\vee$. The septal and ventral components of $\vec{q}_{t_l}, \vec{q}_{t_l+1}, \ldots, \vec{q}_{t_{l+1}}$ are used as the input to the trained HMMs resulting from Section 4.4.1. The most likely state sequences are thus estimated by maximizing the probabilities given the current HMM parameters and the observations, which are given by

$$\kappa_s^I(t_l) = \max_{\wp_s^I(t_l)} \left(\mathrm{P}(\wp_s^I(t_l)|\mathrm{O}_s^I(t_l), \gamma_s^I)\right),$$

$$\kappa_s^{II}(t_l) = \max_{\wp_s^{II}(t_l)} \left(\mathrm{P}(\wp_s^{II}(t_l)|\mathrm{O}_s^{II}(t_l), \gamma_s^{II})\right),$$

$$\kappa_v^I(t_l) = \max_{\wp_v^I(t_l)} \left(\mathrm{P}(\wp_v^I(t_l)|\mathrm{O}_v^I(t_l), \gamma_v^I)\right),$$

$$\kappa_v^{II}(t_l) = \max_{\wp_v^{II}(t_l)} \left(\mathrm{P}(\wp_v^{II}(t_l)|\mathrm{O}_v^{II}(t_l), \gamma_v^{II})\right),$$

$$l = 0, 1, \ldots, L - 1. \tag{27}$$

The obtained state sequences according to Equation (27) are stored in the four feature libraries.

4.4.3 DTW-Based Classifier

By employing Viterbi algorithm, one may estimate the most likely state sequences given the HMMs obtained from Section 4.4.1 and the test data. The test data's septal components are used to estimate two most likely state sequences which maximize the probability for the HMM γ_s^I (trust Septal data) or the HMM γ_s^{II} (non-trust Septal data). It yields

$$\hat{\kappa}_s^I(t_l) = \max_{\wp_s^I(t_l)} \left(\mathrm{P}(\wp_s^I(t_l)|\mathrm{O}_s^I(t_l), \gamma_s^I)\right),$$

$$l = 0, 1, \ldots, L - 1,$$

$$\hat{\kappa}_s^{II}(t_l) = \max_{\wp_s^{II}(t_l)} \left(\mathrm{P}(\wp_s^{II}(t_l)|\mathrm{O}_s^{II}(t_l), \gamma_s^{II})\right),$$

$$l = 0, 1, \ldots, L - 1, \tag{28}$$

where $\hat{\kappa}_s^I(t_l)$ and $\hat{\kappa}_s^{II}(t_l)$, $l = 0, 1, \ldots, L-1$ denote the most likely state sequences given the test data $O_s(t_l) \overset{\text{def}}{=} \left[\bar{s}_{t_l}, \bar{s}_{t_l+1}, \ldots, \bar{s}_{t_{l+1}}\right]$ with respect to γ_s^I and γ_s^{II}. On the other hand, the test data's ventral tegmental components are used to estimate two most likely state sequences which maximize the probability for the HMM γ_v^I (trust Ventral data) or the HMM γ_v^{II} (non-trust Ventral data). It yields

$$\kappa_v^I(t_l) = \max_{\wp_v^I(t_l)} \left(\mathrm{P}(\wp_v^I(t_l) | \mathrm{O}_v^I(t_l), \gamma_v^I)\right),$$

$$l = 0, 1, \ldots, L-1,$$

$$\kappa_v^{II}(t_l) = \max_{\wp_v^{II}(t_l)} \left(\mathrm{P}(\wp_v^{II}(t_l) | \mathrm{O}_v^{II}(t_l), \gamma_v^{II})\right),$$

$$l = 0, 1, \ldots, L-1. \tag{29}$$

Similarly, $\hat{\kappa}_v^I(t_l)$ and $\hat{\kappa}_v^{II}(t_l)$, $l = 0, 1, \ldots, L-1$ denote the most likely state sequences given the test data $O_v(t_l) \overset{\text{def}}{=} \left[\bar{v}_{t_l}, \bar{v}_{t_l+1}, \ldots, \bar{v}_{t_{l+1}}\right]$ with respect to γ_v^I and γ_v^{II}.

It is obvious that the lengths of the estimated state sequences are not necessarily equal to the lengths of the stored state sequences in the feature libraries. Thus, the DTW algorithm [71, 72] should be employed to compute the minimum distances between an estimated state sequence and all the stored state sequences in the corresponding feature library. For instance, the trust Septal feature library corresponds to the estimated state sequence $\hat{\kappa}_s^I(t_l), l = 0, 1, \ldots, L-1$.

Given a state sequence $\hat{\kappa}(t_l) \in \{\hat{\kappa}_s^I(t_l), \quad \hat{\kappa}_s^{II}(t_l), \quad \hat{\kappa}_v^I(t_l), \quad \hat{\kappa}_v^{II}(t_l)\}$ calculated from the test data and an arbitrary state sequence $\kappa(t_h) \in \{\kappa_s^I(t_h), \quad \kappa_s^{II}(t_h), \quad \kappa_v^I(t_h), \quad \kappa_v^{II}(t_h)\}$ picked from the corresponding feature library, the *minimum distance* between them is defined as

$$\eta\left(\hat{\kappa}(t_l), \kappa(t_h)\right) \stackrel{\text{def}}{=} \min\left(\frac{1}{\mathcal{L}}\sum_{\varrho=1}^{\mathcal{L}} w_\varrho\right), \tag{30}$$

where

$$\hat{\kappa}(t_l) \stackrel{\text{def}}{=} [\hat{\rho}(t_l), \hat{\rho}(t_l+1), \dots, \hat{\rho}(t_{l+1})],$$

$$\hat{\kappa}(t_h) \stackrel{\text{def}}{=} [\hat{\rho}(t_h), \hat{\rho}(t_h+1), \dots, \hat{\rho}(t_{h+1})]. \tag{31}$$

Note that

$$\hat{\rho}(t_k) \in S, \rho(t_k) \in S,$$

$$0 \leq k \leq L-1. \tag{32}$$

Moreover,

$$\max(t_{l+1} - t_l + 1, t_{h+1} - t_h + 1) \leq \mathcal{L} \leq t_{l+1} - t_l + t_{h+1} - t_h + 1 \tag{33}$$

and $\mathcal{L}$ is an integer; $w_\varrho, \varrho = 1, 2, \dots, \mathcal{L}$ arise from a set of entries in the matrix $\mathcal{W} \in \mathcal{R}(t_{h+1} - t_h + 1) \times (t_{l+1} - t_l + 1)$ which is defined as

$\mathcal{W} \stackrel{\text{def}}{=}$

$$\begin{bmatrix} \sqrt{\hat{\rho}^2(t_l) - \hat{\rho}^2(t_h)} & \sqrt{\hat{\rho}^2(t_l+1) - \hat{\rho}^2(t_h)} & \cdots & \sqrt{\hat{\rho}^2(t_{l+1}) - \hat{\rho}^2(t_h)} \\ \sqrt{\hat{\rho}^2(t_l) - \hat{\rho}^2(t_h+1)} & \sqrt{\hat{\rho}^2(t_l+1) - \hat{\rho}^2(t_h+1)} & \cdots & \sqrt{\hat{\rho}^2(t_{l+1}) - \hat{\rho}^2(t_h+1)} \\ \vdots & \vdots & \ddots & \vdots \\ \sqrt{\hat{\rho}^2(t_l) - \hat{\rho}^2(t_{h+1})} & \sqrt{\hat{\rho}^2(t_l+1) - \hat{\rho}^2(t_{h+1})} & \dots & \sqrt{\hat{\rho}^2(t_{l+1}) - \hat{\rho}^2(t_{h+1})} \end{bmatrix}.$$

(31)

Note that w_ϱ is selected from $\mathcal{W}$ according to specific criteria (see [43]). Since four kinds of minimum distances are computed with respect to trust Septal data, trust Ventral data, non-trust Septal data, and non-trust Ventral data, the average of the former two distances is undertaken and compared to the average of the latter two distances. Then, the test data is classified as either trust or non-trust data subject to the minimum between these two averages.

5. Experimental Results and Discussion

5.1 Preliminary Analysis of Hidden Markov Model

To evaluate our proposed new technique, experiments based on real fMRI data are employed to test its effectiveness. The parameters adopted in this experiment are stated as follows. All fMRI data used in our experiments were recorded from the first player (see Figure 6).

Four-dimensional volume time series were acquired by resampling the functional time series data of the first player. The cubic voxel used in re-sampling is $3 \times 3 \times 3$ mm^3. The coordinates for septal and ventral tegmental areas (each area corresponds to a voxel) in Talairach space are (6, 11, 4) and (0, −10, −10), respectively. For all games, 286 volume images per game were recorded. Players made nine decisions (either trust or non-trust) in each game. Consequently, there were totally 729 detected events which have been recorded (88 players and 9 decisions for each player). Subject to the decision-making time instance, the aforementioned images were approximately equally divided into three data subsets, say $\mathcal{D}_I$, $\mathcal{D}_{II}$, and $\mathcal{D}_{III}$. Using the *multifold cross-validation* technique [73], one among these three data sets was used as the test data in turn while the other two data sets were used as the training data. For example, when $\mathcal{D}_I$ was employed as the test data, $\mathcal{D}_{II}$ and $\mathcal{D}_{III}$ were used as the training data set one and the training data set two, respectively (labeled as "fMRI training data1" and "fMRI training data2" in Figure 16).

Different numbers of states N in the HMMs (5, 10, 15, 20, 25, 30) were also investigated in these experiments. Figure 17 illustrates the classification accuracies for these three groups of data ($\mathcal{D}_I$, $\mathcal{D}_{II}$, and $\mathcal{D}_{III}$). In Figure 18, $\mathcal{D}_I$ was clustered using different numbers of clusters (10, 15, and 20). Each class of clustered times series were employed as the input

of the classifier. The classification accuracy measure $\hbar$ used to generate Figure 17 and Figure 18 is defined as $\hbar \stackrel{\text{def}}{=} \frac{\Gamma_c}{\Gamma}$, where Γ_c is the number of times when the player's decision

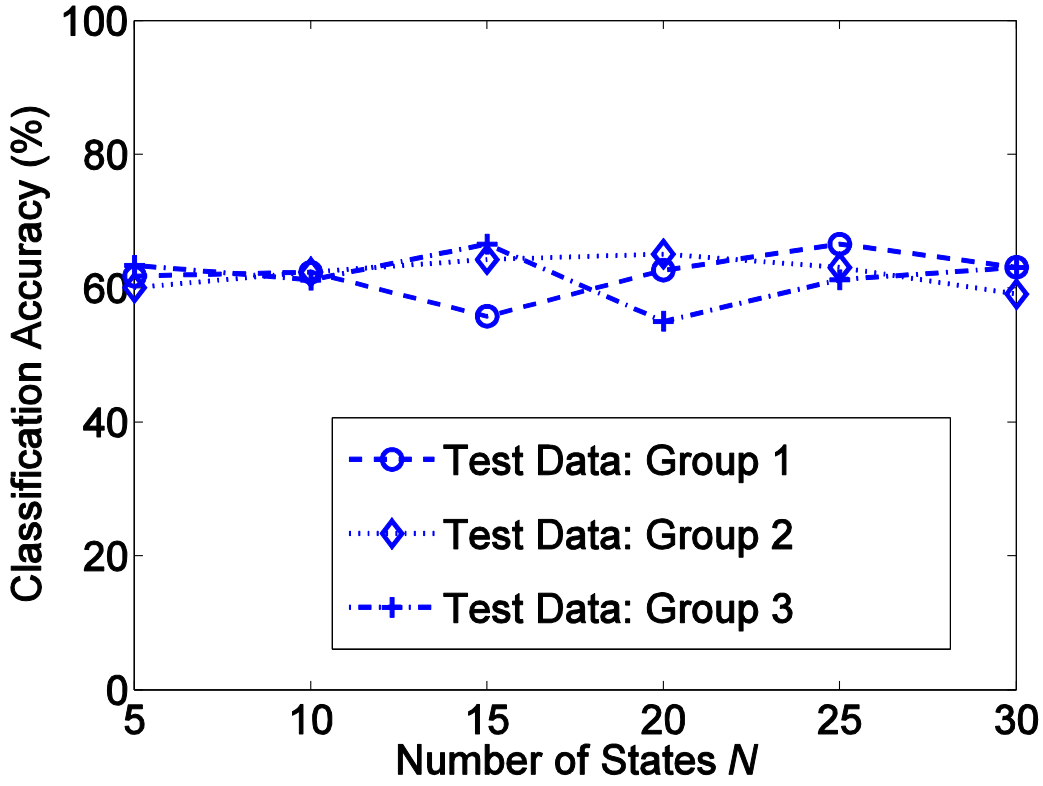

Figure 17. Classification accuracy with respect to the number of states $\boldsymbol{N}$ in HMMs. Three randomly chosen groups of data ($\boldsymbol{\mathcal{D}_I}$, $\boldsymbol{\mathcal{D}_{II}}$, and $\boldsymbol{\mathcal{D}_{III}}$) are employed in this experiment.

is correctly predicted using the fMRI data. Γ is the total number of detected events (decisions). For each data subset $\mathcal{D}_I$, $\mathcal{D}_{II}$ and $\mathcal{D}_{III}$, we have $\Gamma = 240$.

5.2 Classification Results for Speech Data in Comparison

For comparison, audio data files obtained from an open-source class project by Professor Lawrence Rabiner's Digital Signal Processing short course in Summer 2008 (see [74]) were classified using linear classification, SVM and HMM. Of these audio files, 43 contained various male or female voices speaking the number "one" while 46 of the files

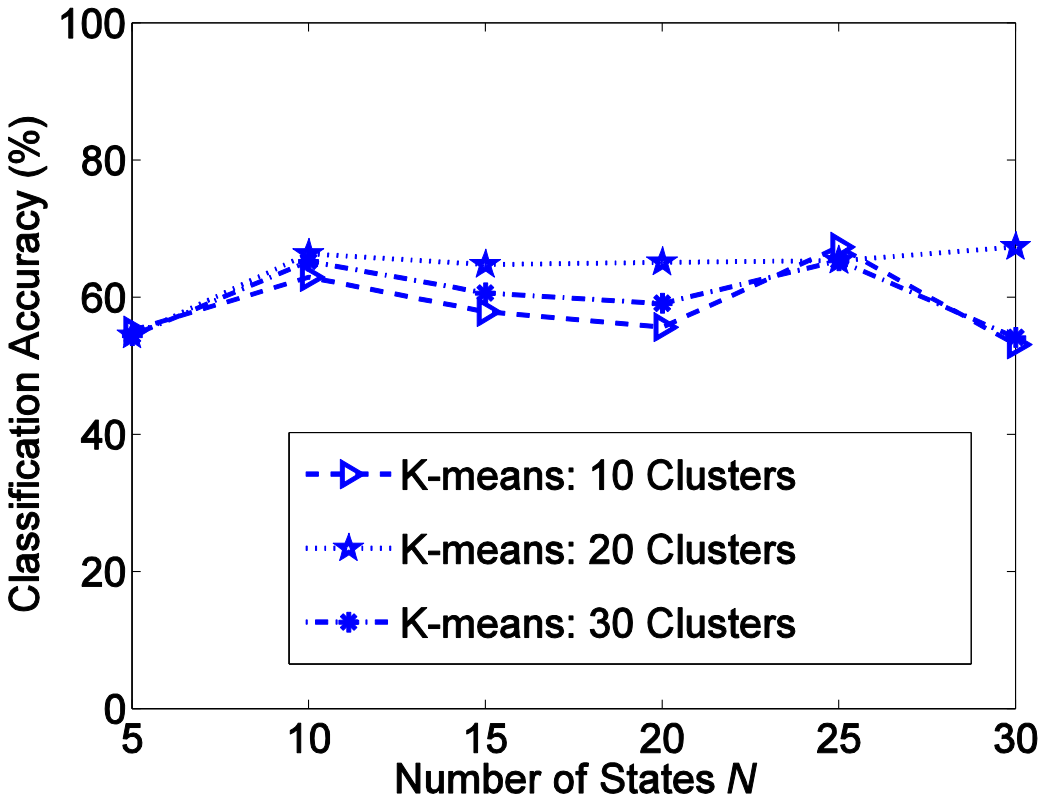

Figure 18. Classification accuracy with respect to the number of states $\boldsymbol{N}$ in HMMs. The test data $\boldsymbol{\mathcal{D}_I}$ are clustered using different $\boldsymbol{K}$ values when the K-means method is implemented.

contained various male or female voices speaking the number "two". These files were combined in sequence. The signals had previously been sampled to the minimum sound period and formatted for MATLAB (© 1994-2013 The MathWorks, Inc.). The files were pre-processed to remove the effects of bias and scaled to reduce inter-subject variations in amplitude.

For classification, the audio dataset was trained and tested with each of the aforementioned classification methods using the *leave-one-out* and *leave-half-out* cross-validation techniques. To calculate the classification rate, the number of correct classifications was divided by the total number of classifications. For the leave-one-out

cross-validation method, the linear classifier and the SVM classified the data into the correct group (trust or non-trust) 92.13% and 97.75% of the time while the HMM model classified the data correctly 92.13% of the time. This exceptional performance by the SVM with leave-one-out may be attributed to the setup of the dataset and the nature of SVMs. Given the setup of the dataset, the classification rates with the leave-half-out technique was much lower, as expected, at 64.30% for the linear classifier, 65.32% for the SVM and 65.91% for the HMM. Detailed results are provided in Figure 19.

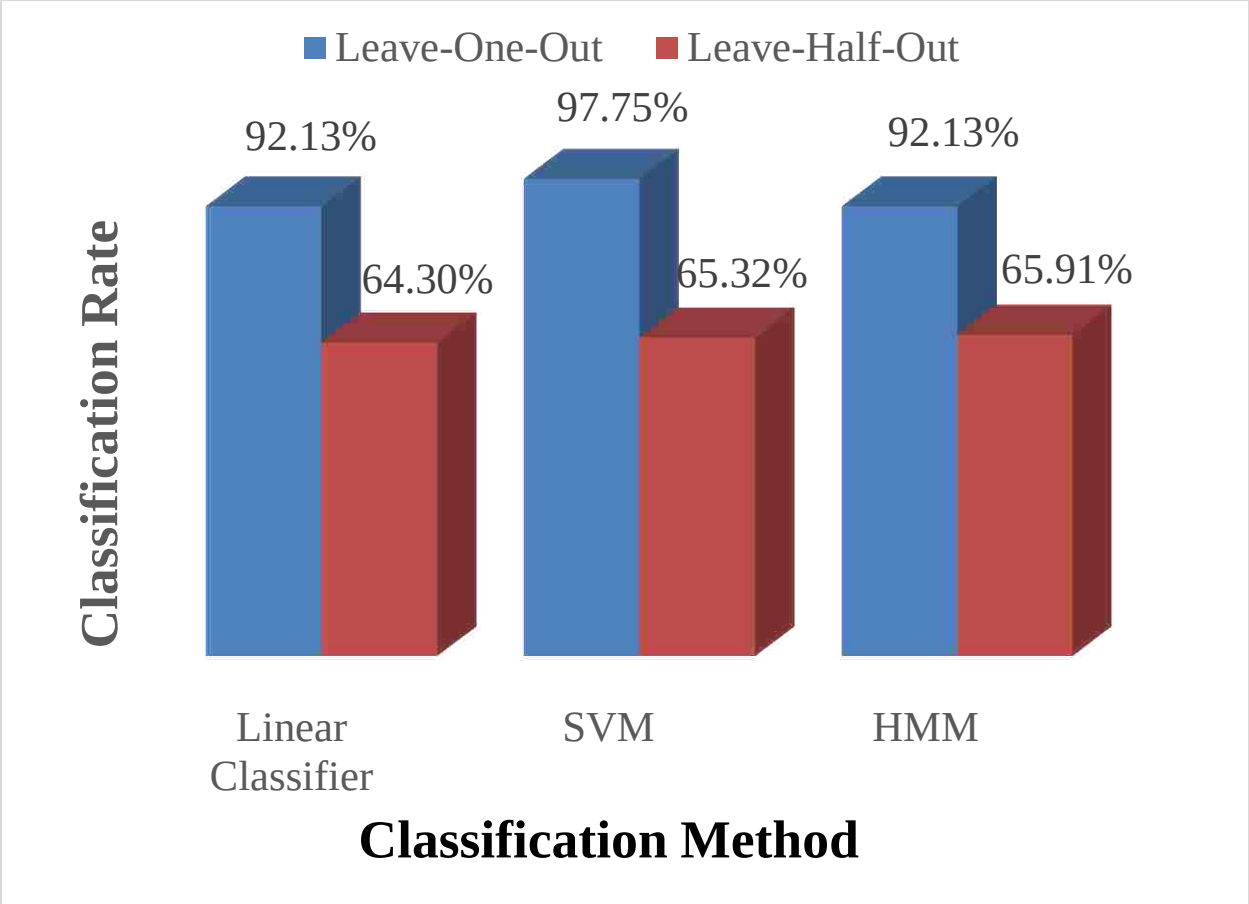

Figure 19. Classification rates with sample speech dataset using leave-one-out and leave-half-out cross-validation techniques for various classification methods including linear classifier, SVM and HMM.

5.3 Classification Results for fMRI Data in Comparison

During feature extraction, prior to extracting ROI-specific time series, for each subject, the mean was subtracted from the raw data to reduce the effects of any bias introduced and the mean-removed data was further divided by the standard deviation to reduce inter-subject variations in amplitude. Following pre-processing, the fMRI dataset was trained and tested with each method using the leave-one-out and leave-half-out cross-validation techniques for each of the four ROIs, i.e. PcC, SA, VTA, striatum, SA and VTA combined, and all ROIs. The classification rates for each cross-validation technique and method (linear classifier, SVM, and HMM) separated by ROI are listed in detail in Figure 20 and Figure 21 with corresponding tables.

With the leave-one-out technique, a basic linear classifier yielded a classification rate between 56% and 61% for individual ROIs and more than 65% for combined ROIs. The SVM classifier yielded results slightly better than the linear classifier ranging between 63% and 66%. The SVM classification results for combined ROIs were not obtained due to ambiguous errors. However, the HMM algorithm consistently achieved a classification rate of about 84% for each ROI individually and combined ROIs.

In contrast, the linear classifier yielded classification rates between 66% and 73% for individual ROIs with the leave-half-out technique. Again, the SVM classifier yielded results slightly better than the linear classifier with classification rates ranging between 67% and 77%. Accordingly, the classification rates for HMM were greater than those of the linear classifier and SVM, but the rates slightly decreased from the leave-one-out technique with individual ROIs (82% to 83%) and slightly increased with an increasing number of ROIs (85% to 86%).

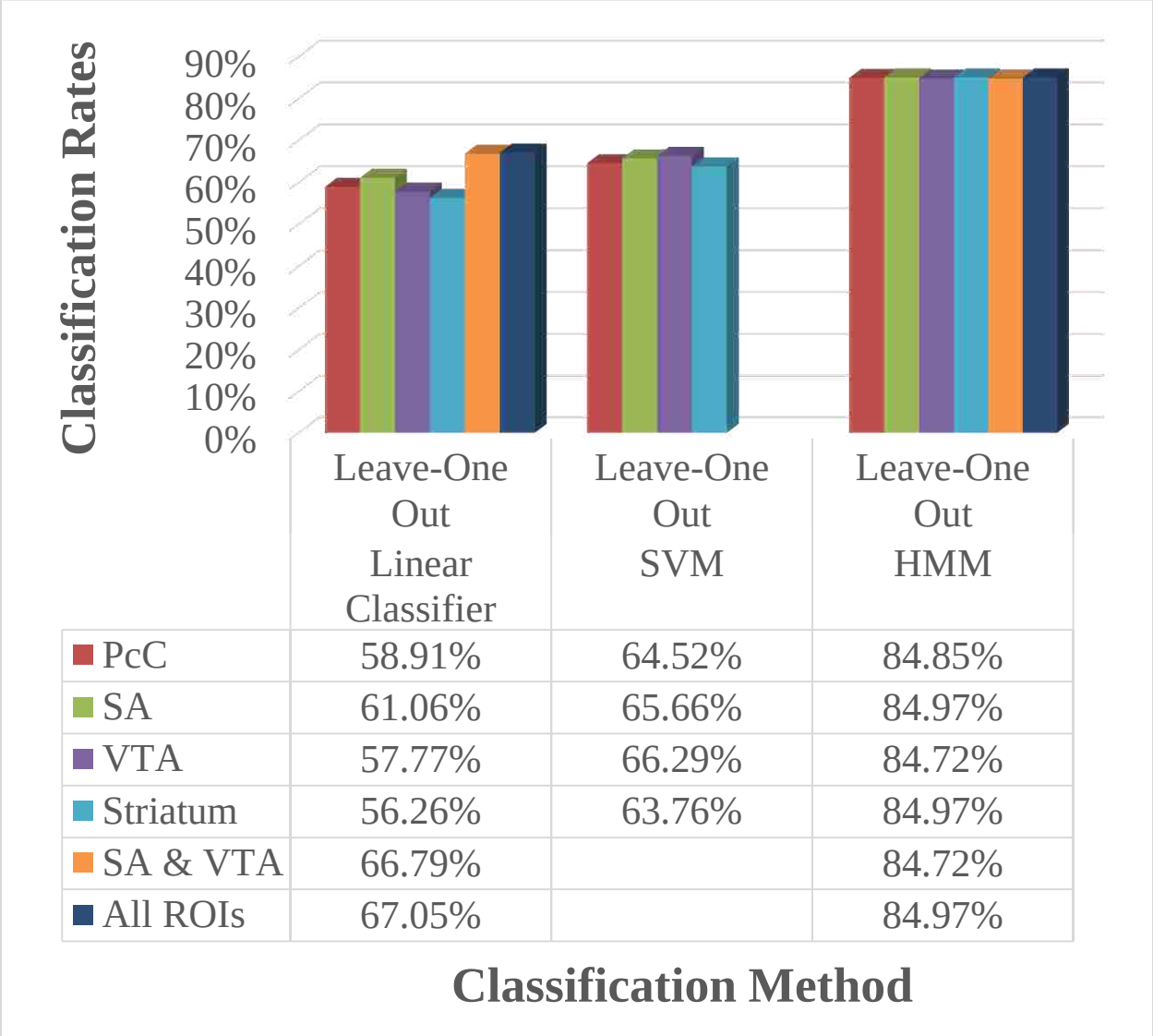

Figure 20. Classification rates for the fMRI dataset from the voluntary reciprocal trust experiment using the leave-one-out cross-validation technique with various classification methods including linear classifier, SVM (with RBF kernels and SMO method) and HMM.

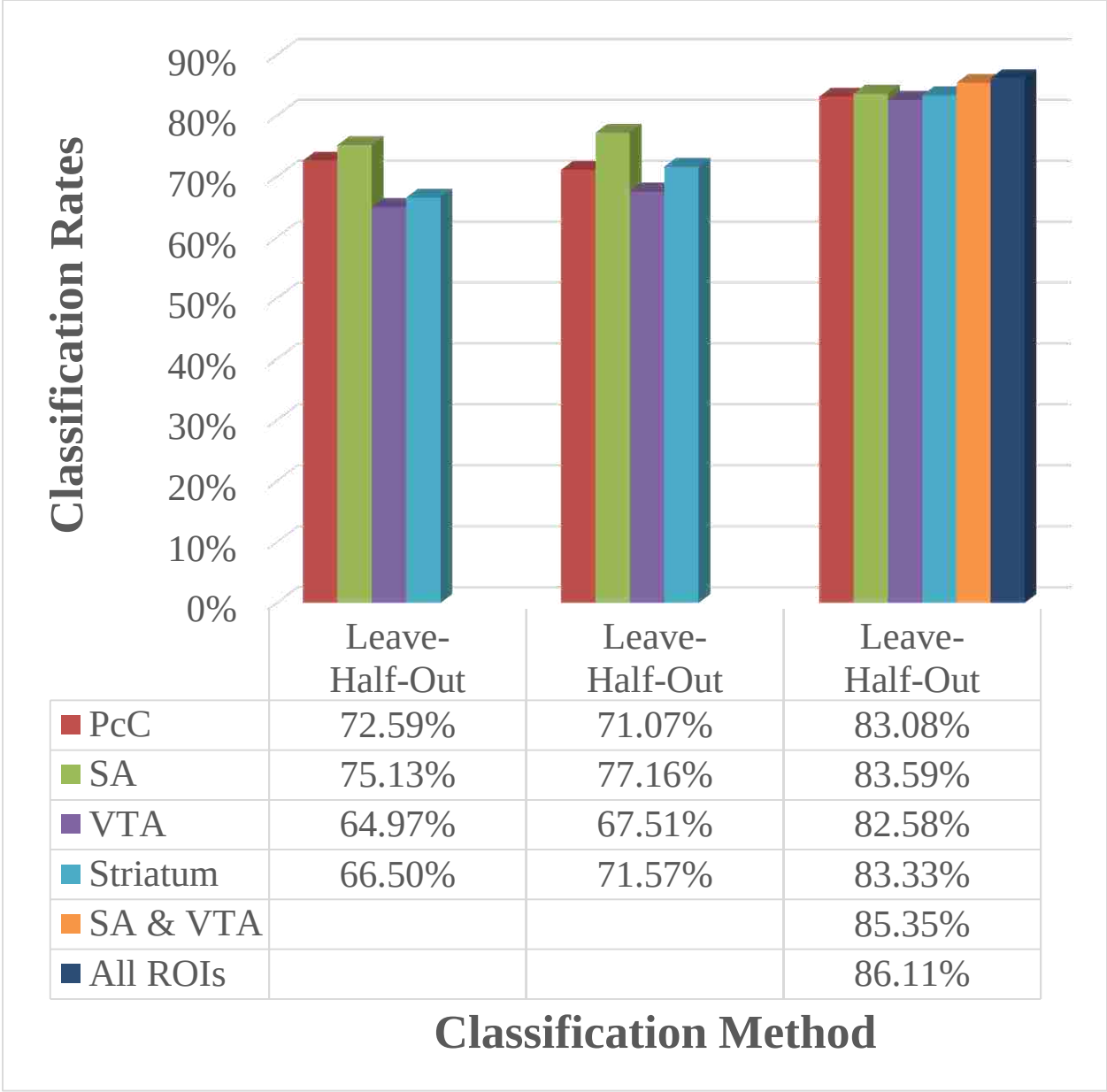

Figure 21. Classification rates for the fMRI dataset from the voluntary reciprocal trust experiment using the leave-half-out cross-validation technique with various classification methods including linear classifier, SVM (with RBF kernels and SMO method) and HMM.

6. Conclusion

This dissertation research investigates the off-line psychological analysis related to voluntary reciprocal trust games using fMRI time series. The Talairach coordinates for the paracingulate cortex, septal area, ventral tegmental area and striatum in the brain are specified to be associated with human's trust behaviors and mentalizing. Hidden Markov models are proposed and compared to other advanced signal processing techniques including linear classification, SVM (with both polynomial and RBF kernels and both SMO and QP methods) to train the fMRI data acquired from these brain regions and extract the essential features for the trust/non-trust prediction. In comparison, the experimental results demonstrate that the HMMs can be adopted as a better paradigm to predict the psychological trust activities reflected by the neural responses recorded by fMRI. Additionally, extracting the specific decision period and clustering the continuous time series proved to increase the classification accuracy by almost 20%.

For further investigation, it would be interesting to use the information about partners to explore the data more in depth especially within the building and maintenance stages. Also, although a similar spatiotemporal response pattern is observed across ROIs, a comparison of additional Talaraich coordinates within the ROIs may yield a different result. After brief exploration, it may be beneficial to investigate the cost-benefit of the leave-half-out cross-validation technique in comparison to the leave-one-out method in that it may save computational time but in the tradeoff of classification rate. A step in another direction may be to observe the classification rates for different tasks and types of acquisition methods. For technology transfer, in the case of a non-invasive measure of motor skills, it may be applied in prosthetics.

References

[1] E. A. DeYoe, P. Bandettini, J. Neitz, D. Miller, and P. Winans, "Functional magnetic resonance imaging (FMRI) of the human brain," *Journal of Neuroscience Methods,* vol. 54, pp. 171-187, 1994.

[2] F. Krueger, K. McCabe, J. Moll, N. Kriegeskorte, R. Zahn, M. Strenziok, *et al.*, "Neural correlates of trust," in *Proc Natl Acad Sci U S A,* vol. 104, pp. 20084-9, Dec 11 2007.

[3] Aristotle, "The Complete Works of Aristotle," in *Politics: Book II* vol. 2, ed. Princeton: Princeton University Press, 1984.

[4] A. Vinciarelli, M. Pantic, D. Heylen, C. Pelachaud, I. Poggi, F. D'Errico, *et al.*, "Bridging the Gap between Social Animal and Unsocial Machine: A Survey of Social Signal Processing," *IEEE Transactions on Affective Computing,* vol. 3, pp. 69-87, 2012.

[5] A. Vinciarelli, M. Pantic, and H. Bourlard, "Social signal processing: Survey of an emerging domain," *Image and Vision Computing,* vol. 27, pp. 1743-1759, 2009.

[6] S. Sherman. (1992, September 21, 1992) ARE STRATEGIC ALLIANCES WORKING? For many companies, success is elusive. The best alliances allow for lots of flexibility and are breaking new ground in the etiquette of corporate power sharing. *Fortune*. Available: http://money.cnn.com/magazines/fortune/fortune_archive/1992/09/21/76881

[7] A. Vinciarelli and M. Pantic, "Techware: www.sspnet.eu: A Web Portal for Social Signal Processing [Best of the Web]," *IEEE Signal Processing Magazine,* vol. 27, pp. 142-144, 2010.

[8] A. Pentland, "Social Signal Processing [Exploratory DSP]," *IEEE Signal Processing Magazine,* vol. 24, pp. 108-111, 2007.

[9] N. Ambady and R. Rosenthal, "Thin slices of expressive behavior as predictors of interpersonal consequences: A meta-analysis," *Psychological Bulletin,* vol. 111, pp. 256-274, 1992.

[10] R. Adolphs, "COGNITIVE NEUROSCIENCE: Cognitive neuroscience of human social behaviour," *Nature Reviews Neuroscience*, vol. 4, p. 165, 2003.

[11] A. A. Salah, M. Pantic, and A. Vinciarelli, "Recent developments in social signal processing," in *2011 IEEE International Conference on Systems, Man, and Cybernetics (SMC), ,* 2011, pp. 380-385.

[12] P. M. Brunet, H. Donnan, G. McKeown, E. Douglas-Cowie, and R. Cowie, "Social signal processing: What are the relevant variables? And in what ways do they relate?," in *3rd International Conference on Affective Computing and Intelligent Interaction and Workshops, 2009. ACII 2009.*, 2009, pp. 1-6.

[13] A. Vinciarelli, "Capturing order in social interactions [Social Sciences]," *IEEE Signal Processing Magazine*, vol. 26, pp. 133-152, 2009.

[14] R. J. P. de Figueiredo, "Cognitive signal processing: An emerging technology for the prediction of behavior of complex human/machine systems," in *International Conference on Communications, Circuits and Systems, 2009. ICCCAS 2009.*, 2009, pp. 1-2.

[15] V. Rozgic, X. Bo, A. Katsamanis, B. Baucom, P. G. Georgiou, and S. Narayanan, "Estimation of ordinal approach-avoidance labels in dyadic interactions: Ordinal logistic regression approach," in *Acoustics, Speech and Signal Processing (ICASSP), 2011 IEEE International Conference on*, 2011, pp. 2368-2371.

[16] A. Vinciarelli, M. Pantic, Herv, #233, Bourlard, and A. Pentland, "Social signal processing: state-of-the-art and future perspectives of an emerging domain," presented at the Proceedings of the 16th ACM international conference on Multimedia, Vancouver, British Columbia, Canada, 2008.

[17] A. Vinciarelli, H. Salamin, and M. Pantic, "Social Signal Processing: Understanding social interactions through nonverbal behavior analysis," in *IEEE Computer Society Conference on Computer Vision and Pattern Recognition Workshops, 2009. CVPR Workshops 2009.*, 2009, pp. 42-49.

[18] F. Krueger, J. Grafman, and K. McCabe, "Neural correlates of economic game playing," *Philosophical Transactions of the Royal Society B: Biological Sciences*, vol. 363, pp. 3859-3874, December 12, 2008 2008.

[19] J. Von Neumann and O. Morgenstern, *Theory of games and economic behavior*. Princeton: Princeton University Press, 1944.

[20] J. Von Neumann and O. Morgenstern, *Theory of games and economic behavior*. Princeton, N.J.; Woodstock: Princeton University Press, 2007.

[21] P. R. Montague, G. S. Berns, J. D. Cohen, S. M. McClure, G. Pagnoni, M. Dhamala*, et al.*, "Hyperscanning: Simultaneous fMRI during Linked Social Interactions," *NeuroImage,* vol. 16, pp. 1159-1164, 2002.

[22] D. M. Niyazov, A. J. Butler, Y. M. Kadah, C. M. Epstein, and X. P. Hu, "Functional magnetic resonance imaging and transcranial magnetic stimulation: Effects of motor imagery, movement and coil orientation," *Clinical Neurophysiology,* vol. 116, pp. 1601-1610, 2005.

[23] N. F. Ramsey, H. Hoogduin, and J. M. Jansma, "Functional MRI experiments: acquisition, analysis and interpretation of data," *European Neuropsychopharmacology,* vol. 12, pp. 517-526, 2002.

[24] Z. Jiang, C. Huafu, F. Fang, and L. Wei, "Convolution Power Spectrum Analysis for fMRI Data Based on Prior Image Signal," *IEEE Transactions on Biomedical Engineering,* , vol. 57, pp. 343-352, 2010.

[25] A. Kundu and G. C. Chen, "An integrated hybrid neural network and hidden Markov model classifier for sonar signal classification," in *1995 International Conference on Acoustics, Speech, and Signal Processing, 1995. ICASSP-95.*, 1995, pp. 3587-3590 vol.5.

[26] G. de Marco, B. Devauchelle, and P. Berquin, "Brain functional modeling, what do we measure with fMRI data?," *Neuroscience Research,* vol. 64, pp. 12-19, 2009.

[27] X. Wei, L. Yi-Ou, L. Hualiang, T. Adali, and V. D. Calhoun, "On ICA of complex-valued fMRI: Advantages and order selection," in *IEEE International Conference on Acoustics, Speech and Signal Processing, 2008. ICASSP 2008.*, 2008, pp. 529-532.

[28] B. P. Rogers, V. L. Morgan, A. T. Newton, and J. C. Gore, "Assessing functional connectivity in the human brain by fMRI," *Magnetic Resonance Imaging,* vol. 25, pp. 1347-1357, 2007.

[29] A. Ganapathiraju, J. Hamaker, and J. Picone, "Applications of Support Vector Machines to Speech Recognition," *IEEE Transactions on Signal Processing,* vol. 52, pp. 2348-2355, 2004.

[30] S. Chakrabartty and G. Cauwenberghs, "Forward Decoding Kernel Machines: A Hybrid HMM/SVM Approach to Sequence Recognition," *Lecture notes in computer science.*, pp. 278-292, 2002.

[31] W. H. Yu, H. Hovik, and T. Chen, "A hidden Markov support vector machine framework incorporating profile geometry learning for identifying microbial RNA in tiling array data," *Bioinformatics,* vol. 26, pp. 1423-30, Jun 1 2010.

[32] Y. Altun, I. Tsochantaridis, and T. Hofmann, "Hidden Markov Support Vector Machines," *International Workshop Then Conference Machine Learning,* vol. 20, pp. 3-10, 2003.

[33] A. Castellani, D. Botturi, M. Bicego, and P. Fiorini, "Hybrid HMM/SVM model for the analysis and segmentation of teleoperation tasks," in *IEEE International Conference Robotics and Automation, 2004. Proceedings. ICRA '04.*, 2004, pp. 2918-2923 Vol.3.

[34] B. Q. Huang, C. J. Du, Y. B. Zhang, and M. T. Kechadi, "A Hybrid HMM-SVM Method for Online Handwriting Symbol Recognition," in *Sixth International Conference on Intelligent Systems Design and Applications, 2006. ISDA '06.*, 2006, pp. 887-891.

[35] Q. Shao, C. Shao, and J. Kang, "Hybrid SVM/HMM Method for Tool Wear Intelligence Measure in Cutting Process," in *2010 International Conference on Information Management, Innovation Management and Industrial Engineering (ICIII)*, 2010, pp. 525-529.

[36] E. Zarrouk, Y. Benayed, and F. Gargouri, "Hybrid SVM/HMM model for the recognition of Arabic triphones-based continuous speech," in *2013 10th International Multi-Conference on Systems, Signals & Devices (SSD)*, 2013, pp. 1-7.

[37] S. Qiang, S. Cheng, and F. Changjian, "Identification of nonstationary time series based on SVM-HMM method," in *IEEE International Conference on Service Operations and Logistics, and Informatics, 2008. IEEE/SOLI 2008.* 2008, pp. 293-298.

[38] S. Guangshun and Z. Yang, "An Improved SVM-HMM Based Classifier for Online Recognition of Handwritten Chemical Symbols," in *2010 Chinese Conference on Pattern Recognition (CCPR)*, 2010, pp. 1-5.

[39] L. Shuai-Shi, T. Yan-Tao, and L. Dong, "New research advances of facial expression recognition," in *2009 International Conference on Machine Learning and Cybernetics*, 2009, pp. 1150-1155.

[40] P. Kumawat, A. Khatri, and B. Nagaria, "Offline Handwriting Recognition Using Invariant Moments and Curve Let Transform with Combined SVM-HMM Classifier," in *2013 International Conference on Communication Systems and Network Technologies (CSNT)*, 2013, pp. 144-148.

[41] W. Bin, Y. Shanping, L. Yuegang, and F. Changjian, "Rolling Bearing Faults Diagnosis Method Based on SVM-HMM," in *2010 International Conference on Measuring Technology and Mechatronics Automation (ICMTMA)*, 2010, pp. 295-298.

[42] Z. Yang, S. Guangshun, and W. Kai, "A SVM-HMM Based Online Classifier for Handwritten Chemical Symbols," in *2010 20th International Conference on Pattern Recognition (ICPR)*, 2010, pp. 1888-1891.

[43] S. A. Mahmoud and S. O. Olatunji, "Handwritten Arabic numerals recognition using multi-span features & Support Vector Machines," in *2010 10th International Conference on Information Sciences Signal Processing and their Applications (ISSPA)*, 2010, pp. 618-621.

[44] L. R. Rabiner, "A tutorial on hidden Markov models and selected applications in speech recognition," in *Proceedings of the IEEE,* vol. 77, pp. 257-286, 1989.

[45] L. R. Rabiner and B. H. Juang, *Fundamentals of speech recognition*. Englewood Cliffs, N.J.: PTR Prentice Hall, 1993.

[46] A. Cohen, "Hidden Markov models in biomedical signal processing," in *Engineering in Medicine and Biology Society, 1998. IEEE Proceedings of the 20th Annual International Conference*, 1998, pp. 1145-1150 vol.3.

[47] L. Yong, D. Guoya, G. Xiaorong, G. Shangkai, G. Manling, and Y. Weili, "Single trial EEG classification during finger movement task by using hidden Markov

models," in *IEEE EMBS Conference on Neural Engineering, 2005. Conference Proceedings. 2nd International*, 2005, pp. 625-628.

[48] H. Jin, L. Huaming, and T. Jindong, "Real-time Daily Activity Classification with Wireless Sensor Networks using Hidden Markov Model," in *IEEE 29th Annual International Conference of the Engineering in Medicine and Biology Society, 2007. EMBS 2007.*, 2007, pp. 3192-3195.

[49] G. G. Georgoulas, C. D. Stylios, G. Nokas, and P. P. Groumpos, "Classification of fetal heart rate during labour using hidden Markov models," in *Neural Networks, 2004. Proceedings. 2004 IEEE International Joint Conference on*, 2004, pp. 2471-2475 vol.3.

[50] T. Shimokawa, K. Kinoshita, K. Miyagawa, and T. Misawa, "A brain information-aided intelligent investment system," *Decision Support Systems*.

[51] T. Shimokawa, K. Suzuki, T. Misawa, and K. Miyagawa, "Predictability of investment behavior from brain information measured by functional near-infrared spectroscopy: A bayesian neural network model," *Neuroscience*, vol. 161, pp. 347-358, 2009.

[52] F. De Martino, F. Gentile, F. Esposito, M. Balsi, F. Di Salle, R. Goebel, *et al.*, "Classification of fMRI independent components using IC-fingerprints and support vector machine classifiers," *NeuroImage*, vol. 34, pp. 177-194, 2007.

[53] F. De Martino, G. Valente, N. Staeren, J. Ashburner, R. Goebel, and E. Formisano, "Combining multivariate voxel selection and support vector machines for mapping and classification of fMRI spatial patterns," *NeuroImage*, vol. 43, pp. 44-58, 2008.

[54] K.-R. Muller, "An Introduction to Support Vector Machines and Other Kernel-Based Learning Methods (Book)," *IEEE Transactions on Neural Networks*, vol. 13, p. 787, 2002.

[55] M.-F. Lucas, A. Gaufriau, S. Pascual, C. Doncarli, and D. Farina, "Multi-channel surface EMG classification using support vector machines and signal-based wavelet optimization," *Biomedical Signal Processing and Control*, vol. 3, pp. 169-174, 2008.

[56] L. B. a. C.-j. Lin, "Support Vector Machine Solvers," 2006.

[57] B. H. Boyle, *Support Vector Machines : Data Analysis, Machine Learning, and Applications*. New York: Nova Science Publishers, 2011.

[58] I. Tsochantaridis, T. Hofmann, T. Joachims, and Y. Altun, "Support vector machine learning for interdependent and structured output spaces," presented at the International Conference on Machine Learning, 2004.

[59] L. P. V. S. M. F. Landini, *Advanced image processing in magnetic resonance imaging*. Boca Raton, FL: CRC/Taylor & Francis, 2005.

[60] R. Goebel, F. Esposito, and E. Formisano, "Analysis of functional image analysis contest (FIAC) data with brainvoyager QX: From single-subject to cortically aligned group general linear model analysis and self-organizing group independent component analysis," *Hum Brain Mapp,* vol. 27, pp. 392-401, May 2006.

[61] J. Moll, F. Krueger, R. Zahn, M. Pardini, R. de Oliveira-Souza, and J. Grafman, "Human fronto–mesolimbic networks guide decisions about charitable donation," in *Proceedings of the National Academy of Sciences,* vol. 103, pp. 15623-15628, October 17, 2006 2006.

[62] D. M. Amodio and C. D. Frith, "Meeting of minds: the medial frontal cortex and social cognition," *Nat Rev Neurosci,* vol. 7, pp. 268-277, 04//print 2006.

[63] A. Aron, H. Fisher, D. J. Mashek, G. Strong, H. Li, and L. L. Brown, "Reward, Motivation, and Emotion Systems Associated With Early-Stage Intense Romantic Love," *Journal of Neurophysiology*, vol. 94, pp. 327-337, July 1, 2005 2005.

[64] N. Christianini, and J. Shawe-Taylor, *An Introduction to Support Vector Machines and Other Kernel-Based Learning Methods*. Cambridge, UK: Cambridge University Press, 2000.

[65] R. O. Duda, P. E. Hart, and D. G. Stork, *Pattern classification*. New York: Wiley, 2001.

[66] T. Hastie, R. Tibshirani, and J. Friedman, *The Elements of Statistical Learning*, Second ed. New York: Springer, 2008.

[67] F. Jelinek, *Statistical methods for speech recognition / Frederick Jelinek*: Cambridge, Mass. : MIT Press, c1997., 1997.

[68] X. Hui, W. Junjie, and C. Jian, "K-Means Clustering Versus Validation Measures: A Data-Distribution Perspective," *Systems, Man, and Cybernetics, Part B: Cybernetics, IEEE Transactions on*, vol. 39, pp. 318-331, 2009.

[69] R. Johnson, Jr., P. Schniter, T. J. Endres, J. D. Behm, D. R. Brown, and R. A. Casas, "Blind equalization using the constant modulus criterion: a review," *Proceedings of the IEEE*, vol. 86, pp. 1927-1950, 1998.

[70] M. A. Ferrer, I. G. Alonso, and C. M. Travieso, "Influence of initialisation and stop criteria on HMM based recognisers," *Electronics Letters*, vol. 36, pp. 1165-1166, 2000.

[71] E. J. K. a. M. J. Pazzani, "Scaling up Dynamic Time Warping for Datamining Applications," *In Proc. 6th Int. Conf. on Knowledge Discovery and Data Mining*, pp. 285 - 289, 2000.

[72] E. J. Keogh and M. J. Pazzani, "Scaling up dynamic time warping for datamining applications," presented at the Proceedings of the sixth ACM SIGKDD international conference on Knowledge discovery and data mining, Boston, Massachusetts, USA, 2000.

[73] S. Haykin, *Neural Networks: A Comprehensive Foundation*: Prentice Hall, 1999.

[74] L. Rabiner. (2011, November 7). *Digital Signal Processing*. Available: http://cronos.rutgers.edu/~lrr/

Appendix A

Charisma Edwards <cedwa15@tigers.lsu.edu>

Permission to Use Figures from Publication

Charisma D. Edwards <cedwa15@tigers.lsu.edu> Fri, May 25, 2012 at 12:58 PM
To: Edgar DeYoe <deyoe@mcw.edu>

Dr. DeYoe,

Thank you so much! I will be certain to reference the article in each figure caption.

Charisma

--
Charisma D. Edwards
Doctoral Student
Electrical Engineering
Louisiana State University
Mobile: (832) 527-8404
E-mail: cedwa15@tigers.lsu.edu

On Fri, May 25, 2012 at 12:01 PM, Edgar DeYoe <deyoe@mcw.edu> wrote:

> Charisma,
>
> sorry for the delay. here's a PDF. Feel free to use any figures that you would like, though please include a reference to the paper within
>
> the figure caption of each one you use.
>
> Thanks,
>
> Ted DeYoe
>
> ---
> Edgar A DeYoe, PhD
> Dept. Radiology, MEB Neurolab
> Medical College of Wisconsin
> 8701 Watertown Plank Rd.
> Milwaukee WI, 53226
> Email: deyoe@mcw.edu
> Office Phone: 414-456-4920
> Lab Phone: 414-456-4919
> Fax: 414-456-6382
>
> "In the mountains, we forget to count the days"
> Chinese proverb
>
> *The information contained in this communication may be confidential and is intended only for the use of the recipient(s) named above, and may be legally privileged. If the reader of this message is not the intended recipient, you are hereby notified that any dissemination, distribution, or copying of this communication, or any of its contents is*

strictly prohibited. If you have received this communication in error, please return it to the sender immediately and delete the original message and any copy from your computer system. If you have any questions concerning this message, please contact the sender.

From: [illegible]
Sent: [illegible]
To: [illegible]
Subject: [illegible]

Good afternoon Dr. DeYoe,

Recently, I requested from Elsevier permission to use up to 10 figures from your journal article below for my dissertation:

> DeYoe, E.A., et al., *Functional magnetic resonance imaging (FMRI) of the human brain.* Journal of Neuroscience Methods, 1994. **54**(2): p. 171-187.

I would like to request permission from you as well. However, I have not located an electronic version anywhere. Can you recommend somewhere to obtain an electronic copy?

Thank you so much in advance for your time and assistance!

Kindest regards,
Charisma D. Edwards
Doctoral Student
Electrical Engineering
Louisiana State University
Mobile: (832) 527-8404
E-mail: cedwa15@tigers.lsu.edu

——— Forwarded message ———
From: **Copyright Clearance Center** <rightslink@marketing.copyright.com>
Date: Fri, May 11, 2012 at 4:24 PM
Subject: Thank you for your RightsLink / Elsevier transaction
To: cedwa15@lsu.edu

RightsLink | Copyright Clearance Center

Thank You For Your Order!

Dear Miss. Charisma Edwards,

Thank you for placing your order through Copyright Clearance Center's RightsLink service. Elsevier has partnered with RightsLink to license its content. This notice is a confirmation that your order was successful.

Your order details and publisher terms and conditions are available by clicking the link below:
http://s100.copyright.com/CustomerAdmin/PLF.jsp?ID=2012050_1336771458065

Order Details
Licensee: Charisma D Edwards
License Date: May 11, 2012
License Number: 2906121314065
Publication: Journal of Neuroscience Methods
Title: Functional magnetic resonance imaging (FMRI) of the human brain
Type Of Use: reuse in a thesis/dissertation
Total: 0.00 USD

To access your account, please visit https://myaccount.copyright.com.

Please note: Online payments are charged immediately after order confirmation; invoices are issued daily and are payable immediately upon receipt.

To ensure we are continuously improving our services, please take a moment to complete our customer satisfaction survey.

B.1>4.2

+1-877-622-5543 / Tel: +1-978-646-2777
customercare@copyright.com
http://www.copyright.com

Appendix B

Copyright and License to Publish

Beginning with articles submitted in Volume 106 (2009) the author(s) retains copyright to individual articles, and the National Academy of Sciences of the United States of America retains an exclusive license to publish these articles and holds copyright to the collective work. Volumes 90–105 copyright © (1993–2008) by the National Academy of Sciences. Volumes 1–89 (1915–1992), the author(s) retains copyright to individual articles, and the National Academy of Sciences holds copyright to the collective work.

The PNAS listing on the Sherpa RoMEO publisher copyright policies & self-archiving detail pages can be found here (http://www.sherpa.ac.uk/romeo/search.php?id=94&la=en&fIDnum=|).

Requests for Permission to Reprint

Requests for permission should be made in writing. For the fastest response time, please send your request via e-mail to PNASPermissions@nas.edu (mailto:PNASPermissions@nas.edu). If necessary, requests may be faxed to 202-334-2739 or mailed to:

PNAS Permissions Editor
[illegible] Fifth Street, NW
NAS 340
Washington, DC 20001 USA

Anyone may, without requesting permission, use original figures or tables published in PNAS for noncommercial and educational use (i.e., in a review article, in a book that is not for sale) provided that the original source and the applicable copyright notice are cited.

(/content/current)

Current Issue (/content/current)

E-mail Alerts (/site/misc/PNASalerts.xhtml)

Subscribe (/site/subscriptions/index.xhtml)

RSS (/site/aboutpnas/rss.xhtml)

Other PNAS Media

Image Gallery (/site/media/imagegallery.xhtml)

Video Library (/site/media/videolibrary.xhtml)

Follow Us on Twitter (https://twitter.com/PNASNews)

Find Us on Facebook (http://www.facebook.com/pages/PNAS/18252365099)

Vita

Charisma D. Edwards is a doctoral candidate in Electrical Engineering at Louisiana State University (LSU) in Baton Rouge, Louisiana. Her research is in digital signal processing with a focus in biomedical signal classification, which was inspired by her work in neuroimaging at Emory University in Atlanta, Georgia. Through her experiences as a pre-college and college freshman instructor with LSU College of Engineering Diversity Programs and as a NSF K-12 Fellow through the LSU Gordon A. Cain Center, she developed a strong interest in and passion for K-12 outreach and engineering education. Charisma gained recognition as a leader of the Black Graduate and Professional Student Association at LSU and was nominated for Graduate Student Leader of the Year in 2010. Currently, she serves as coordinator for tutoring and leadership initiatives for the NSF/Innovation through Institutional Integration (I^3) grant project to bridge numerous programs across campus and Baton Rouge metropolitan community in the Office of Strategic Initiatives (OSI). Through OSI, she was awarded her first grant as a Co-Principal Investigator. Ms. Edwards earned her B.S. in Engineering from Clark Atlanta University in 2004 and her M.S. in Electrical Engineering from LSU in 2007. Charisma hopes to finally receive her Ph.D. in Electrical Engineering from LSU in December 2013.